THE ASTROPHYSICAL JOURNAL, 470:864–881, 1996 October 20

JHKL PHOTOMETRY AND THE *K*-BAND LUMINOSITY FUNCTION AT THE GALACTIC CENTER

R. D. BLUM,[1,2,3] K. SELLGREN,[1,4] AND D. L. DEPOY[1]
Department of Astronomy, The Ohio State University, 174 West 18th Avenue, Columbus, OH, 43210
Received 1996 January 24; accepted 1996 May 10

ABSTRACT

J, *H*, *K*, and *L* photometry for the stars in the central $\sim 2'$ (~ 5 pc) of the Galaxy are presented. Using the observed $J-H$, $H-K$, and $K-L$ colors and assumed intrinsic colors, we determine the interstellar extinction at 2.2 μm (A_K) for approximately 1100 individual stars. The mean A_K ($=3.3$ mag) is similar to previous results, but we find that the reddening is highly variable, and some stars are likely to be seen through $A_K > 6$ mag. The dereddened *K*-band luminosity function points to a significantly brighter component to the stellar population (>1.5 mag at *K*) than found in the stellar population in Baade's window, confirming previous work done at lower spatial resolution. The *observed* flux of all Galactic center stars with estimated K_0 (dereddened magnitude) ≤ 7.0 mag is $\sim 25\%$ of the total in the $2' \times 2'$ field.

Our observations confirm the recent finding that several bright M stars in the Galactic center are variable. Our photometry also establishes the near-infrared variability of the M1-2 supergiant, IRS 7.

Subject headings: dust, extinction — Galaxy: center — Galaxy: stellar content — infrared: stars — stars: luminosity function, mass function

1. INTRODUCTION

The Galactic center (GC) stellar cluster is unique in the Milky Way. The central core of stars in the Galaxy is an extremely dense composite of older red giants and young, massive stars that exhibit energetic winds through emission-line spectra. Since the earliest work on the GC, investigators have been trying to isolate these young and old(er) components. In their discovery paper of the GC stellar cluster, Becklin & Neugebauer (1968) discussed a dominant extended infrared source and an infrared point source. Infrared maps at increasingly higher angular resolution resolved the extended infrared source into a cluster of stars (Becklin & Neugebauer 1975; Allen, Hyland, & Jones 1983; Storey & Allen 1983) and identified the infrared point source of Becklin & Neugebauer (1968) as the brightest star in this cluster. Infrared spectroscopy of individual GC sources (Treffers et al. 1976; Neugebauer et al. 1976; Wollman, Smith, & Larson 1982; Hall, Kleinmann, & Scoville 1982; Lebofsky, Rieke, & Tokunaga 1982, hereafter LRT) found that they fell into two broad groups, sources with and without CO absorption at 2.3 μm, a signature of late-type giants and supergiants. Lacy, Townes, & Hollenbach (1982) suggested that a group of O and B stars could produce the observed excitation in the diffuse ionized gas in one of the first papers calling for a massive, young population to exist at the GC. LRT identified four stars as late-type supergiants including the brightest 2 μm source, IRS 7. Using these as tracers of a star formation episode, they postulated that a starburst ($2 \times 10^3\ M_\odot$ within the central ~ 5 pc) occurred approximately 10^7 yr ago. Subsequent discoveries of one to two dozen emission-line stars (Allen, Hyland, & Hillier 1990; Krabbe et al. 1991) have increased the estimates of the starburst intensity to $1.6 \times 10^4\ M_\odot$ (Krabbe et al. 1995).

Clearly, the GC represents a unique region of star formation in the Galaxy. We need to account for the delivery and subsequent collapse of large amounts of gas in the central region. The massive stars currently identified in the GC have lifetimes too short to have moved far from their birthplaces (LRT; Morris 1993). We must also understand the role of collisional processes that may result in unusual star formation (Morris 1993) in the extremely dense GC region ($\gtrsim 10^7\ M_\odot\ \mathrm{pc}^{-3}$; Bailey 1980; Eckart et al. 1993, 1995), especially since stellar collisions are likely to occur (Phinney 1989).

Star formation in the GC, despite its unique history, can be studied by the same techniques used in other star formation regions: determination of the distribution of stellar masses, ages, and compositions. As a first step, we present *J*, *H*, *K*, and *L* photometry of the stellar population in the central $\sim 2'$ (~ 5 pc for a GC distance of 8 kpc; Reid 1993). These data are used to investigate the observed color-magnitude diagram and the dereddened *K*-band luminosity function. Our *K*-band luminosity function confirms the excess of bright stars relative to the well-studied bulge field, Baade's window (BW; $l,\ b = 0°,\ -4°$), pointed out previously by Lebofsky & Rieke (1987), Rieke (1987, 1993), Haller & Rieke (1989), and Haller (1992). The present data are of higher spatial resolution and reach fainter magnitudes than these previous studies.

Of these excess bright stars, the blue emission-line stars (Forrest et al. 1987; Allen et al. 1990; Krabbe et al. 1991; Libonate et al. 1995; Blum, Sellgren, & DePoy 1995b; Blum, DePoy, & Sellgren 1995a; Krabbe et al. 1995; Tamblyn et al. 1996) have been associated with an epoch of star formation $\lesssim 10^7$ yr ago, while the brighter, cool stars (LRT; Sellgren et al. 1987; Krabbe et al. 1995) may be associated with either the most recent epoch or with somewhat older ones ($\sim 10^8$ yr) as pointed out by Haller (1992) and Krabbe et al. (1995). A companion paper to this one

[1] Visiting Astronomer, Cerro Tololo Inter-American Observatory, National Optical Astronomy Observatories, which are operated by the Association of Universities for Research in Astronomy, Inc., under cooperative agreement with the National Science Foundation.
[2] Hubble Fellow.
[3] Current address: University of Colorado, JILA, Campus Box 440, Boulder, CO 80309.
[4] Alfred P. Sloan Research Fellow.

(Blum, Sellgren, & DePoy 1996, hereafter Paper II) presents K-band spectra for some of the brightest cool stars in the GC. The near-infrared photometry and interstellar extinction estimates presented here are important to the analysis of the 2.2 μm spectra presented in Paper II. This combination of photometry and 2.2 μm spectra allows us to begin to delineate the stellar components resulting from these different putative star formation epochs.

2. OBSERVATIONS AND DATA REDUCTION

The primary data set for the GC observations was obtained on the nights of 1993 July 11–13 on the 4 m telescope at the Cerro Tololo Inter-American Observatory (CTIO) using the Ohio State Infrared Imager and Spectrometer (OSIRIS). OSIRIS is described by DePoy et al. (1993a). All basic data reduction procedures were accomplished using IRAF.[5]

J ($\lambda \approx 1.25$ μm, $\Delta\lambda \approx 0.24$ μm), H ($\lambda \approx 1.65$ μm, $\Delta\lambda \approx 0.30$ μm), and K ($\lambda \approx 2.2$ μm, $\Delta\lambda \approx 0.40$ μm) images were obtained for the ~central 2′ of the Galaxy using OSIRIS at $\sim 0\farcs4$ pixel^{-1} during the night of 1993 July 13. The total exposure times were 320, 70, and 50 s at J, H, and K, respectively. Because of a small region of hot pixels on the OSIRIS NICMOS III detector, the GC was offset 21″ west of center to place it on a clean region of the 256 × 256 chip. The GC frames were taken as a series with telescope offsets of 5″–10″ made in between exposures to account for individual bad pixels. Each of the eight J, seven H, and five K frames was sky subtracted with an image taken 500″–600″ off the GC and ratioed by a dome flat-field image. The seeing was approximately 1″.0 FWHM. We find a plate scale of $0\farcs390$ pixel^{-1} $\pm$ $0\farcs007$ pixel by adopting the positions tabulated in Krabbe et al. (1995) for a number of bright, well separated GC stars (IRS 1W, 6E, 9, 13, 16NE).

Secondary data used to investigate possible variable stars and derive K magnitudes for a small number of saturated stars on the primary K images were obtained on 1993 May 11, 1993 July 13, and 1995 April 24. In 1993 May we obtained H and K images of the GC with OSIRIS on the Perkins Telescope at Lowell Observatory near Flagstaff, Arizona. The K image was obtained with a ~1% neutral density filter. The plate scale was $\sim 1\farcs6$ pixel^{-1}. We obtained narrow-band images of the GC on 1993 July 13 with OSIRIS on the 4 m telescope at CTIO (same plate scale as the primary data). Two $\Delta\lambda/\lambda \sim 1\%$ filters ($\lambda \approx 2.19$ μm, $\lambda \approx 2.27$ μm) were employed. A set of J images was kindly obtained for us on 1995 April 24 by J. A. Frogel, again using OSIRIS at Lowell Observatory. These images were obtained at $\sim 0\farcs6$ pixel^{-1} plate scale.

2.1. *Photometry*

2.1.1. *Analysis*

The photometry in our primary data set was flux calibrated using seven stars of known brightness on the CTIO/CIT photometric system from a single field in BW (Frogel & Whitford 1987, hereafter FW87). These bright stars (B143, B145, B158, B159, B162, B163, and B169, as denoted on the list in FW87) were analyzed with aperture photometry, and an aperture correction relating the instrumental and published magnitudes for the flux standards was computed for each filter. A second aperture correction relating the flux in this aperture to a GC frame instrumental magnitude (instrumental magnitudes for the GC frames were obtained with DAOPHOT; see below) was calculated using between five and eight stars on the GC frames. All aperture photometry used 5 pixel radius circular apertures. For the BW standards, the seeing was approximately 1″ to 1″.5. The 5 pixel aperture was large enough that corrections due to seeing differences were insignificant. The stars used in computing the second aperture correction on the GC frames were chosen to be relatively bright and uncrowded. The sum of these two corrections was then applied to the GC photometry. The photometric uncertainty (error in the mean) due to the two corrections is $\pm$0.028, 0.030, and 0.024 mag at J, H, and K, respectively.

The narrow-band data in our secondary data set (used to obtain photometry for saturated stars in the primary K data set, see below) were flux calibrated using the derived magnitudes for seven bright GC stars from Table 1 (IRS 6E, 11, 14NE, 15NE, 16NE, 28, and OSU C2). These stars are represented roughly equally by hot and cool stars (Table 1). We find OSIRIS K and OSIRIS narrow band agree to $\pm$0.04 mag (standard deviation in the mean, average of the two narrow-band filters). The secondary H and K images (used to investigate variability only, see below) were calibrated using the magnitudes for stars IRS 19, IRS 22, star 74, and star 124 (Table 1); these four stars agree to $\pm$0.06 and $\pm$0.08 mag at H and K, respectively (standard deviation in the mean). The secondary J images from 1995 April (also used to investigate variability) were calibrated using the same BW stars as given above for the primary data set (uncertainty in calibration: $\pm$0.04 mag.) For these secondary J images, magnitudes for IRS 7 were obtained by 5 pixel radius aperture photometry.

The primary J, H, and K images and secondary narrow-band, H, and K images were analyzed individually with DAOPHOT (Stetson 1987) in order to obtain the stellar photometry. The particular version of DAOPHOT employed is one modified by Jon Holtzman of Lowell Observatory and integrated into the Ohio State/Lowell Observatory VISTA image reduction and analysis software program. There are two main differences between the version of DAOPHOT, as employed here, and the original. First is the use of a new grouping routine that is more computationally efficient for extremely crowded fields. In this routine, each star is analyzed separately with all of its neighbors which lie within a critical radius. For the GC frames, a critical radius of 10–12 pixels was used resulting in groups with approximately up to 20 stars. Second, the background was determined locally and was a free parameter in the profile fitting. Each set of frames at a given wavelength was analyzed with a point-spread function defined by the same two or three stars.

The resulting DAOPHOT instrumental magnitudes for the primary data set were then combined to form average J, H, and K lists. The photometry lists from different frames were merged by matching the coordinates of stars on the lists. After making initial estimates of frame-to-frame offsets from bright stars, the coordinate lists were matched in an iterative procedure which typically resulted in residual offsets between frames of 0.00 ± 0.20 pixel. Magnitudes from the individual lists were averaged, and only stars detected on two or more frames were kept in the final J, H, or K lists. Figure 1 shows the DAOPHOT error as function of J, H, and K magnitude. Brighter stars have DAOPHOT

[5] IRAF is distributed by the National Optical Astronomy Observatories.

TABLE 1

GALACTIC CENTER OBSERVED PHOTOMETRY

ID	Name	$\Delta\alpha$ (arcsec)[a]	$\Delta\delta$ (arcsec)[a]	K	$J-K$	$H-K$	$K-L$	Notes
1.....		−40.07	−8.01	10.40 ± 0.08	...	...	...	
2.....		−38.31	−22.60	10.27 ± 0.05	...	...	...	
3.....		−37.55	6.96	10.10 ± 0.05	...	...	...	
4.....		−34.38	−18.66	10.36 ± 0.04	6.85 ± 0.07	2.74 ± 0.06	...	
5.....		−29.36	−23.17	10.26 ± 0.03	6.61 ± 0.06	2.62 ± 0.05	...	
6.....		−28.49	−40.40	9.67 ± 0.03	...	...	...	
7.....		−26.91	18.90	9.80 ± 0.03	7.15 ± 0.06	2.76 ± 0.05	...	
8.....		−24.04	18.35	10.24 ± 0.06	6.65 ± 0.07	2.51 ± 0.07	...	
9.....		−23.04	16.43	9.92 ± 0.04	6.29 ± 0.05	2.42 ± 0.05	...	
10.....		−22.97	11.96	10.44 ± 0.04	7.11 ± 0.09	2.99 ± 0.05	...	
11.....		−22.40	41.86	9.22 ± 0.14	...	...	...	
12.....		−21.48	42.24	10.32 ± 0.08	5.34 ± 0.10	1.94 ± 0.11	...	
13.....		−20.12	−32.15	10.06 ± 0.03	7.42 ± 0.07	3.33 ± 0.05	...	H92
14.....		−19.30	25.37	10.48 ± 0.03	6.75 ± 0.05	2.68 ± 0.05	...	
15.....		−17.16	28.26	10.45 ± 0.03	6.27 ± 0.05	2.43 ± 0.05	...	H92
16.....		−16.97	10.34	9.59 ± 0.03	4.78 ± 0.04	1.70 ± 0.04	...	H92
17.....		−16.09	18.45	9.74 ± 0.03	6.07 ± 0.04	2.48 ± 0.05	...	
18.....		−13.72	15.34	10.18 ± 0.04	...	3.16 ± 0.05	...	
19.....		−13.27	−16.88	10.14 ± 0.03	7.57 ± 0.15	3.01 ± 0.05	...	H92
20.....		−10.90	−32.26	10.49 ± 0.04	...	2.52 ± 0.05	...	
21.....		−9.76	−25.81	10.24 ± 0.03	6.07 ± 0.05	2.24 ± 0.05	...	
22.....	BSD WC9	−9.69	−11.54	10.74 ± 0.05	...	2.08 ± 0.07	...	WC9
22.....	BSD WC9	−9.69	−11.54	10.72 ± 0.05	...	...	...	[b]
23.....		−9.59	6.47	9.75 ± 0.03	6.14 ± 0.04	2.31 ± 0.05	...	
24.....		−9.36	−17.17	10.18 ± 0.04	5.53 ± 0.05	2.05 ± 0.06	...	
25.....	AF NWB	−9.11	−8.97	11.67 ± 0.14	...	...	...	[b]
25.....	AF NWB	−9.11	−8.97	11.60 ± 0.09	5.26 ± 0.10	2.37 ± 0.12	...	
26.....	BSD WC9B	−9.08	−11.90	12.07 ± 0.13	...	...	...	[b]
26.....	BSD WC9B	−9.08	−11.90	12.04 ± 0.14	...	1.84 ± 0.18	...	
27.....		−9.05	−34.75	9.02 ± 0.03	...	2.66 ± 0.05	...	
28.....	IRS 11	−8.44	8.03	9.17 ± 0.07	5.95 ± 0.07	1.99 ± 0.08	...	Cool
29.....	AF NW	−8.24	−9.28	11.93 ± 0.17	...	...	...	[b]
29.....	AF NW	−8.24	−9.28	11.85 ± 0.11	5.15 ± 0.13	2.29 ± 0.15	...	He I
30.....	IRS 6WB	−8.17	−4.01	11.51 ± 0.42	...	...	...	[b]
31.....	IRS 6W	−8.12	−4.40	10.26 ± 0.14	...	...	...	[b]
31.....	IRS 6W	−8.12	−4.40	10.22 ± 0.05	5.78 ± 0.06	2.40 ± 0.07	...	
32.....	AF B	−7.79	−13.58	11.24 ± 0.07	5.25 ± 0.09	1.95 ± 0.09	...	
33.....	AF	−7.28	−12.89	10.74 ± 0.09	...	...	...	[b]
33.....	AF	−7.28	−12.89	10.70 ± 0.05	5.12 ± 0.06	2.06 ± 0.06	...	He I
34.....		−7.00	−27.69	10.19 ± 0.06	...	2.36 ± 0.07	...	[a]
35.....	IRS 30	−6.56	0.21	10.68 ± 0.08	...	...	...	
35.....	IRS 30	−6.56	0.21	10.49 ± 0.05	7.11 ± 0.16	2.49 ± 0.11	1.08 ± 0.23	[b]
36.....		−6.47	−22.39	10.37 ± 0.03	5.19 ± 0.04	1.85 ± 0.05	...	
37.....	IRS 30B	−5.87	−0.14	11.15 ± 0.16	...	...	...	
38.....	IRS 6E	−5.53	−5.08	10.06 ± 0.06	...	4.26 ± 0.17	...	WC9
38.....	IRS 6E	−5.53	−5.08	9.80 ± 0.06	...	...	2.96 ± 0.08	[b]
39.....		−5.03	−28.27	10.37 ± 0.04	6.20 ± 0.05	2.37 ± 0.05	...	
40.....		−4.89	−33.81	10.09 ± 0.05	...	...	...	
41.....		−4.50	−30.34	10.14 ± 0.09	...	2.39 ± 0.10	...	
42.....	IRS 13W	−4.45	−7.80	10.96 ± 0.12	...	...	...	Cool
42.....	IRS 13W	−4.45	−7.80	10.61 ± 0.11	...	...	2.87 ± 0.20	[b]
43.....		−4.29	−21.77	10.07 ± 0.03	6.13 ± 0.05	2.29 ± 0.05	...	
44.....	IRS 12NB	−4.16	−13.61	10.10 ± 0.10	5.69 ± 0.11	2.43 ± 0.12	...	
45.....	IRS 2	−4.15	−10.47	10.57 ± 0.06	...	3.65 ± 0.13	...	Cool
45.....	IRS 2	−4.15	−10.47	10.34 ± 0.09	...	...	2.29 ± 0.14	[b]
46.....	IRS 34	−4.13	−4.09	10.75 ± 0.07	...	...	...	He I
46.....	IRS 34	−4.13	−4.09	10.48 ± 0.08	...	2.83 ± 0.16	1.87 ± 0.19	[b]
47.....	IRS 12S	−4.10	−14.63	9.95 ± 0.05	5.85 ± 0.06	2.18 ± 0.06	...	Cool
48.....	IRS 22	−3.90	−31.98	8.03 ± 0.03	5.13 ± 0.04	1.77 ± 0.05	...	[c], Cool
49.....	IRS 2L	−3.87	−9.64	11.68 ± 0.20	...	...	4.37 ± 0.21	[d]
50.....	IRS 12N	−3.86	−12.91	8.58 ± 0.04	6.95 ± 0.05	2.83 ± 0.06	...	[c, e], Cool
50.....	IRS 12N	−3.86	−12.91	8.48 ± 0.05	8.68 ± 0.23	2.88 ± 0.06	0.80 ± 0.18	[b]
51.....		−3.51	−7.21	10.14 ± 0.20	...	...	...	
52.....	IRS 13E	−3.37	−7.51	9.82 ± 0.13	5.71 ± 0.14	2.34 ± 0.14	...	He I
52.....	IRS 13E	−3.37	−7.51	9.60 ± 0.15	...	...	3.21 ± 0.16	[b]
53.....	IRS 3	−2.45	−2.01	11.16 ± 0.11	...	...	...	Red
53.....	IRS 3	−2.45	−2.01	10.79 ± 0.07	...	...	5.52 ± 0.07	[b]
54.....	IRS A7	−2.10	2.71	10.50 ± 0.05	6.17 ± 0.06	2.42 ± 0.07	...	
55.....	IRS 29S	−1.93	−4.91	10.55 ± 0.28	5.90 ± 0.29	2.57 ± 0.29	...	Cool
56.....	IRS 29N	−1.79	−4.41	9.96 ± 0.11	...	...	...	WC9
56.....	IRS 29N	−1.79	−4.41	9.87 ± 0.11	...	...	2.67 ± 0.13	[b]
57.....	IRS 20	−1.45	−11.30	10.61 ± 0.05	5.89 ± 0.07	2.26 ± 0.07	...	Cool

TABLE 1—*Continued*

ID	Name	Δα (arcsec)[a]	Δδ (arcsec)[a]	*K*	*J*−*K*	*H*−*K*	*K*−*L*	Notes
57	IRS 20	−1.45	−11.30	10.56 ± 0.08	...	...	0.69 ± 0.49	[b]
58	F95 J	−1.33	11.60	10.38 ± 0.03	6.15 ± 0.05	2.40 ± 0.05	...	H92, Cool
59	MPE−1.0−3.5	−1.00	−3.76	11.90 ± 0.22	...	...	2.02 ± 0.46	[b], WC9
60	IRS 14SW	−0.73	−15.13	10.15 ± 0.04	6.72 ± 0.07	2.59 ± 0.06	...	Cool
61	IRS 33W	−0.68	−9.22	10.87 ± 0.07	6.07 ± 0.11	2.18 ± 0.10	...	Cool
61	IRS 33W	−0.68	−9.22	10.86 ± 0.11	...	...	1.01 ± 0.34	[b]
62	IRS 15SW	−0.43	5.95	10.39 ± 0.04	5.59 ± 0.05	2.15 ± 0.06	...	He I
63	IRS A11	−0.25	−8.07	10.92 ± 0.12	...	...	2.00 ± 0.18	[b]
63	IRS A11	−0.25	−8.07	10.87 ± 0.06	5.28 ± 0.07	2.05 ± 0.08	...	
64		−0.16	31.53	10.13 ± 0.03	6.53 ± 0.05	2.51 ± 0.05	...	
65	IRS 16NW	−0.08	−4.72	10.03 ± 0.07	...	...	...	[b], He I
65	IRS 16NW	−0.08	−4.72	10.03 ± 0.04	5.01 ± 0.06	2.01 ± 0.06	...	
66	IRS 7	0.15	−0.24	6.40 ± 0.03	6.64 ± 0.04	2.42 ± 0.10	...	[c], [e], Cool
66	IRS 7	0.15	−0.24	6.70 ± 0.10	7.10 ± 0.14	2.60 ± 0.14	2.15 ± 0.14	[b]
67	IRS 33E	0.31	−9.13	10.02 ± 0.05	5.57 ± 0.06	2.21 ± 0.07	...	He I
67	IRS 33E	0.31	−9.13	9.86 ± 0.06	...	...	0.73 ± 0.25	[b]
68	IRS 14NE	0.36	−14.21	9.75 ± 0.04	6.80 ± 0.06	2.64 ± 0.06	...	Cool
69		0.39	−34.01	9.79 ± 0.03	7.02 ± 0.08	2.75 ± 0.05	...	
70	F95 B	0.44	−28.15	9.88 ± 0.06	6.30 ± 0.07	2.49 ± 0.08	...	Cool
71	IRS 16SW	0.67	−7.15	9.60 ± 0.05	5.15 ± 0.06	2.00 ± 0.07	...	He I
71	IRS 16SW	0.67	−7.15	9.34 ± 0.10	...	...	1.30 ± 0.12	[b]
72	F95 A	0.82	−36.34	9.05 ± 0.04	3.74 ± 0.05	1.27 ± 0.05	...	Cool
73		0.90	−7.70	10.03 ± 0.07	5.40 ± 0.08	2.05 ± 0.09	...	
74	IRS 16C	1.12	−5.61	9.86 ± 0.05	5.37 ± 0.06	2.13 ± 0.06	...	He I
74	IRS 16C	1.12	−5.61	9.79 ± 0.05	...	...	1.31 ± 0.09	[b]
75	IRS 15NE	1.38	5.61	8.96 ± 0.04	6.03 ± 0.05	2.41 ± 0.05	...	He I & Cool
76	OSUF 1	1.38	−12.49	11.40 ± 0.08	5.38 ± 0.11	2.18 ± 0.11	...	[f]
76	OSUF 1	1.38	−12.49	11.31 ± 0.14	...	...	...	[b]
77	MPE+1.6−6.8	1.58	−7.21	9.98 ± 0.06	6.00 ± 0.08	2.42 ± 0.08	...	WC9
77	MPE+1.6−6.8	1.58	−7.21	9.88 ± 0.14	...	...	2.00 ± 0.14	[b]
78	IRS 8	1.88	23.90	10.49 ± 0.06	...	...	...	Red
79		2.01	42.73	9.73 ± 0.13	6.60 ± 0.13	2.28 ± 0.13	...	
80	IRS 16CC	2.02	−5.61	10.51 ± 0.11	...	...	1.85 ± 0.16	[b]
80	IRS 16CC	2.02	−5.61	10.20 ± 0.07	5.36 ± 0.09	2.08 ± 0.09	...	He I
81	IRS 21	2.22	−8.83	10.40 ± 0.05	...	...	...	Red
81	IRS 21	2.22	−8.83	10.11 ± 0.06	...	...	3.20 ± 0.06	[b]
82	TAM He1	2.59	−11.82	12.05 ± 0.13	...	...	...	[g], He I
82	TAM He1	2.59	−11.82	12.01 ± 0.19	...	...	...	[b]
83	IRS 16NE	2.89	−4.90	9.01 ± 0.05	5.00 ± 0.06	1.93 ± 0.06	...	He I
83	IRS 16NE	2.89	−4.90	8.99 ± 0.05	...	...	1.44 ± 0.07	[b]
84		3.08	−17.50	9.88 ± 0.04	7.38 ± 0.08	3.06 ± 0.07	...	
85		3.12	−7.23	11.00 ± 0.08	5.08 ± 0.09	2.02 ± 0.10	...	
85		3.12	−7.23	10.95 ± 0.12	...	...	1.41 ± 0.20	[b]
86		3.45	−8.42	11.79 ± 0.13	...	...	...	
87	IRS A19	3.67	−13.25	11.61 ± 0.09	6.94 ± 0.29	...	1.85 ± 0.23	[b]
87	IRS A19	3.67	−13.25	11.18 ± 0.06	...	2.53 ± 0.08	...	
88		5.01	−13.32	10.03 ± 0.18	7.17 ± 0.20	...	...	
89	OSU He1	5.35	−3.01	12.36 ± 0.23	...	...	...	[f], He I
90		5.40	28.38	10.11 ± 0.08	5.82 ± 0.09	1.96 ± 0.09	...	
91	IRS 9	5.42	−12.60	8.53 ± 0.04	6.45 ± 0.05	2.46 ± 0.06	...	[c], [e], Cool
91	IRS 9	5.42	−12.60	8.61 ± 0.03	7.33 ± 0.07	2.24 ± 0.04	1.45 ± 0.04	[b]
92	IRS 1W	5.42	−5.61	8.66 ± 0.04	...	...	3.16 ± 0.07	[b]
92	IRS 1W	5.42	−5.61	8.81 ± 0.04	6.21 ± 0.06	3.13 ± 0.07	...	[c], Red
93		6.63	−6.01	10.70 ± 0.13	5.86 ± 0.18	...	2.14 ± 0.22	[b]
93		6.63	−6.01	10.61 ± 0.13	...	2.37 ± 0.16	...	
94	IRS 10W	6.91	−0.97	10.27 ± 0.06	6.48 ± 0.08	3.13 ± 0.08	...	
94	IRS 10W	6.91	−0.97	10.22 ± 0.07	...	...	3.42 ± 0.07	[b]
95		7.07	−5.21	10.62 ± 0.09	6.04 ± 0.13	...	1.78 ± 0.17	[b]
95		7.07	−5.21	10.46 ± 0.07	...	2.56 ± 0.10	...	
96	IRS 1NE	7.28	−4.33	10.32 ± 0.08	...	...	1.50 ± 0.12	[b]
96	IRS 1NE	7.28	−4.33	10.00 ± 0.07	...	2.50 ± 0.09	...	Cool
97	IRS 1SE	7.49	−6.58	10.28 ± 0.06	...	...	...	[b]
97	IRS 1SE	7.49	−6.58	10.23 ± 0.04	6.66 ± 0.11	2.46 ± 0.06	...	Cool
98	IRS 10EL	8.07	−1.82	10.75 ± 0.09	...	...	4.25 ± 0.09	[d]
99		8.63	−24.83	9.76 ± 0.03	6.50 ± 0.05	2.45 ± 0.05	...	
100		8.80	3.79	10.38 ± 0.04	6.97 ± 0.08	3.92 ± 0.08	...	
101	IRS 10E	8.95	−2.04	10.36 ± 0.06	6.22 ± 0.07	2.17 ± 0.08	...	Cool
102	IRS 28	10.57	−12.09	9.36 ± 0.03	6.94 ± 0.05	2.81 ± 0.05	...	Cool
103	OSU C2	10.82	−5.03	10.10 ± 0.04	6.20 ± 0.06	2.35 ± 0.06	...	Cool
104		11.63	−2.42	10.47 ± 0.04	5.93 ± 0.05	2.21 ± 0.05	...	
105		13.32	−0.66	8.91 ± 0.03	6.28 ± 0.04	2.32 ± 0.05	...	
106		13.45	6.89	10.33 ± 0.03	6.27 ± 0.05	2.41 ± 0.05	...	

TABLE 1—*Continued*

ID	Name	Δα (arcsec)[a]	Δδ (arcsec)[a]	*K*	*J*−*K*	*H*−*K*	*K*−*L*	Notes
107.....		13.72	17.46	10.10 ± 0.03	6.27 ± 0.04	2.35 ± 0.04	...	
108.....	IRS 19	14.43	−25.74	8.22 ± 0.03	6.59 ± 0.04	2.61 ± 0.04	...	[e], Cool
109.....	IRS 18	14.94	−17.40	9.50 ± 0.03	6.36 ± 0.04	2.40 ± 0.04	...	
110.....		15.55	−28.56	10.07 ± 0.04	7.09 ± 0.07	2.95 ± 0.05	...	
111.....		16.55	44.67	10.39 ± 0.04	6.48 ± 0.10	2.24 ± 0.06	...	
112.....	OSU C3	17.09	−11.31	10.73 ± 0.04	...	3.06 ± 0.05	...	Cool
113.....		17.69	−0.87	10.01 ± 0.04	...	2.59 ± 0.07	...	
114.....		18.28	44.62	8.53 ± 0.04	5.81 ± 0.05	2.24 ± 0.05	...	[e]
115.....		20.23	22.67	10.26 ± 0.04	6.14 ± 0.05	2.35 ± 0.05	...	
116.....	OSU C1	20.61	−8.91	10.64 ± 0.04	...	2.53 ± 0.06	...	Cool
117.....		20.67	24.29	10.40 ± 0.04	5.90 ± 0.05	2.25 ± 0.05	...	
118.....		21.42	32.42	10.27 ± 0.03	6.04 ± 0.05	2.31 ± 0.04	...	
119.....		23.26	−25.08	10.38 ± 0.03	6.72 ± 0.06	2.59 ± 0.05	...	
120.....		23.31	−3.24	10.48 ± 0.03	7.00 ± 0.07	2.75 ± 0.05	...	
121.....		23.45	17.26	9.52 ± 0.03	7.13 ± 0.04	2.83 ± 0.04	...	
122.....		26.16	38.74	10.20 ± 0.04	5.67 ± 0.05	2.07 ± 0.05	...	
123.....		28.27	3.63	10.04 ± 0.03	6.88 ± 0.05	2.70 ± 0.04	...	
124.....		32.45	30.92	9.10 ± 0.03	5.34 ± 0.04	1.96 ± 0.04	...	
125.....		33.66	43.92	10.46 ± 0.04	6.39 ± 0.07	2.51 ± 0.06	...	
126.....		35.29	28.04	9.69 ± 0.03	6.86 ± 0.05	2.85 ± 0.05	...	
127.....		35.80	23.53	10.31 ± 0.08	4.91 ± 0.09	1.84 ± 0.10	...	
128.....	IRS 24	36.66	24.18	8.26 ± 0.04	6.36 ± 0.06	2.45 ± 0.05	...	[e], Cool
129.....		38.80	39.37	9.38 ± 0.03	5.47 ± 0.04	2.11 ± 0.05	...	
130.....		38.91	30.15	10.43 ± 0.03	6.10 ± 0.05	2.38 ± 0.05	...	
131.....		40.03	9.35	8.91 ± 0.03	5.31 ± 0.04	1.90 ± 0.05	...	
132.....		40.71	5.48	10.24 ± 0.03	6.23 ± 0.05	2.44 ± 0.05	...	
133.....		40.72	−29.72	9.20 ± 0.03	6.54 ± 0.04	2.63 ± 0.04	...	H92
134.....		40.74	−41.92	10.39 ± 0.03	4.80 ± 0.05	1.66 ± 0.05	...	
135.....	OSU C4	40.82	−4.50	10.67 ± 0.03	...	2.67 ± 0.04	...	Cool
136.....	IRS 23	42.51	8.19	8.62 ± 0.03	6.51 ± 0.04	2.58 ± 0.04	...	[e], Cool
137.....		43.67	40.36	10.18 ± 0.04	5.79 ± 0.05	2.17 ± 0.05	...	
138.....		45.68	11.15	10.40 ± 0.04	6.09 ± 0.05	2.65 ± 0.07	...	H92
139.....		46.08	0.38	9.89 ± 0.03	4.88 ± 0.04	1.75 ± 0.04	...	
140.....		46.84	15.82	9.44 ± 0.03	5.73 ± 0.04	2.16 ± 0.04	...	
141.....		48.27	22.84	10.23 ± 0.03	5.49 ± 0.04	2.01 ± 0.04	...	
142.....		53.16	25.96	9.91 ± 0.03	5.56 ± 0.04	2.14 ± 0.05	...	
143.....		56.84	28.00	9.86 ± 0.03	5.11 ± 0.04	1.88 ± 0.05	...	
144.....		56.93	18.83	10.30 ± 0.04	5.74 ± 0.05	2.15 ± 0.05	...	
145.....		62.56	22.02	10.45 ± 0.03	...	3.28 ± 0.05	...	
146.....		65.70	11.53	10.45 ± 0.03	7.24 ± 0.09	2.89 ± 0.05	...	H92
147.....		67.47	15.40	9.83 ± 0.04	4.63 ± 0.05	1.63 ± 0.05	...	

NOTES—All photometry is from our primary OSIRIS data set unless otherwise noted. The OSIRIS magnitudes include both measurement and calibration uncertainties. The DS91 data include only measurement uncertainty; calibration uncertainty is not included. IRS "A" names are taken from Tamura et al. 1996. Label "B" refers to a (usually) fainter source very close to the primary source. Earlier, lower resolution data likely included both components as a single source. H92 identifies a source of similar brightness and within 2″ of a variable star identified by Haller 1992. F95 refers to sources observed by Figer 1995. Cool identifies a star with CO 2.3 μm absorption based on *K*-band spectra; see LRT, Sellgren et al. 1987, Krabbe et al. 1995, and Paper II. He I identifies a star with 2.06 μm emission based on *K*-band spectra or narrow-band imaging; see Allen et al. 1990, Krabbe et al. 1991, 1995, Libonate et al. 1995, Blum et al. 1995a, and Tamblyn et al. 1996. Red identifies a star with a very red, nearly featureless spectrum based on *K*-band spectra; see Libonate et al. 1995, Blum et al. 1995a, and Krabbe et al. 1995. WC9 identifies a star with C III and C IV emission lines based on *K*-band spectra; see Blum et al. 1995b and Krabbe et al. 1995.

[a] Offset in arcseconds from IRS 7.

[b] Photometry derived from the DePoy & Sharp 1991 data set. *J* and *H* presented from DS91 data only if no value from the OSIRIS data was available (except for IRS 7, 9, and 12N; see note e below); see Appendix. The DS91 data were flux calibrated by assuming the IRS 7 magnitudes of Becklin et al. 1978 which are uncertain by less than ±0.1 mag at each wavelength. Good average agreement between the DS91 photometry and OSIRIS photometry argues that the assumed magnitudes of IRS 7 at the time of the DS91 observations were correct, despite the variability of IRS 7 (see text).

[c] *K* magnitude derived from narrow-band filters at 2.2 μm; see text.

[d] IRS 2 and 10E label the bright sources at *K*. IRS 2L and 10EL label the nearby, but not coincident, bright sources at *L*. For IRS 2L and 10EL we give *K* from OSIRIS and *L* from DS91. IRS 10EL has been identified as a variable star by Tamura et al. 1996 which they call IRS 10*. It may also be the OH/IR star OH 359.946−0.047 in the list of Lindqvist et al. 1992.

[e] See discussion in text on IRS 7, 9, and 12N variability. DS91 magnitudes for IRS 7 are from Becklin et al. 1978 as adopted by DS91. Uncertainty is less than ±0.1 mag at each wavelength. OSIRIS *H* magnitude for IRS 7 is from lower resolution image taken 2 months prior (1993 May 11) to the primary OSIRIS images; see text.

[f] OSU He1 (IRS A22) is an He I emission-line star; OSU F1 (IRS A15) is featureless, both based on unpublished *K*-band spectra.

[g] He I emission-line star identified by Tamblyn et al. 1996 narrow-band photometry, confirmed by our unpublished *K*-band spectrum.

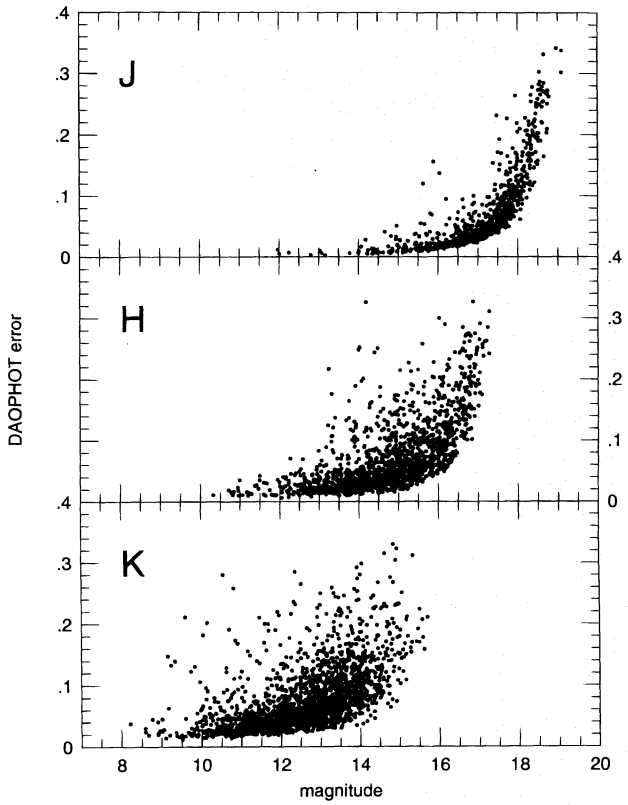

FIG. 1.—DAOPHOT errors for J, H, and K magnitudes. The errors include the uncertainty associated with the aperture corrections to the instrumental magnitudes. For bright stars, typical uncertainties reported from DAOPHOT were similar to the observed scatter between frames. Fainter stars show the effects of crowding as well as photometric uncertainty; see text.

errors that are comparable to the standard deviation in the mean of measurements between different frames. Typical DAOPHOT errors are 0.02, 0.03, and 0.04 mag for $J < 15$, $H < 12$, and $K < 11$, respectively. As Figure 1 suggests, crowding results in larger DAOPHOT errors than the standard deviation in the mean between frames for fainter stars. Average DAOPHOT errors are 0.18, 0.15, and 0.11 mag for all stars with $J > 18$, $H > 16$, and $K > 13$, respectively. The J, H, and K photometry lists were merged in the same way as the individual frame lists with residual spatial offsets between frames of 0.00 ± 0.30 pixels.

Nine stars with $K < 8.6$ mag appear saturated on the primary OSIRIS frames. These saturated stars are represented with photometry from the secondary data set narrow-band images (as indicated in Table 1). However, the saturated stars are all tied to the primary OSIRIS flux scale through the narrow-band images. We will argue later that the GC *dereddened* luminosity function has a brighter component than that in BW. The brightest stars of this component rely on the K magnitudes derived from the narrow-band images. The uncertainty associated with deriving K magnitudes from the narrow-band images could result in systematic differences in magnitudes compared to the OSIRIS primary images. These possible differences will not affect the conclusions drawn later in this paper regarding the K-band luminosity function in the GC because we know the brightest stars were saturated and hence must be generally brighter than the stars in BW. This is most easily seen by comparing the *observed* K for the GC stars to the BW stars with a typical value of extinction to the GC applied (see Fig. 3 and § 2.3). Furthermore, the number of stars not on the primary OSIRIS system is small relative to the total number of stars in the bright component of the GC luminosity function (>110 in either the observed or dereddened luminosity function; see § 3.4).

2.1.2. *Comparison to Other Data*

Color transformations are not available for OSIRIS to the CTIO/CIT system for stars which are as red as those in the GC ($J-K$ up to 7 mag). However, our primary OSIRIS data can be compared to the CTIO/CIT GC photometry derived from the images of DePoy & Sharp (1991, hereafter DS91). DePoy & Sharp originally presented a subset of their photometry for a number of bright stars. We analyzed their images (the co-added, not enhanced, images) in the same way as for the OSIRIS data described above. IRS 7 was used as the PSF star for all the DS91 images. For the J and H frames IRS 7 was nearer the edge of the frame resulting in a PSF with a smaller radius. This could affect the photometry at J and H for the DS91 images; see the Appendix.

Figure 2 shows a comparison of the OSIRIS and DS91 data for 15, 16, and 15 stars at J, H, and K, respectively. Only stars measured at J, H, or K and with J and K magnitudes from DS91 as well were used. Suspected variables (see below) and stars near the edge of the DS91 frames were excluded. Each panel of this figure shows a weighted, least-squares fit as well. The slopes for ΔJ, ΔH, and ΔK versus $(J-K)_{\rm CTIO/CIT}$ are 0.003 ± 0.011, -0.023 ± 0.012, and -0.016 ± 0.009, respectively. Figure 2 suggests no sta-

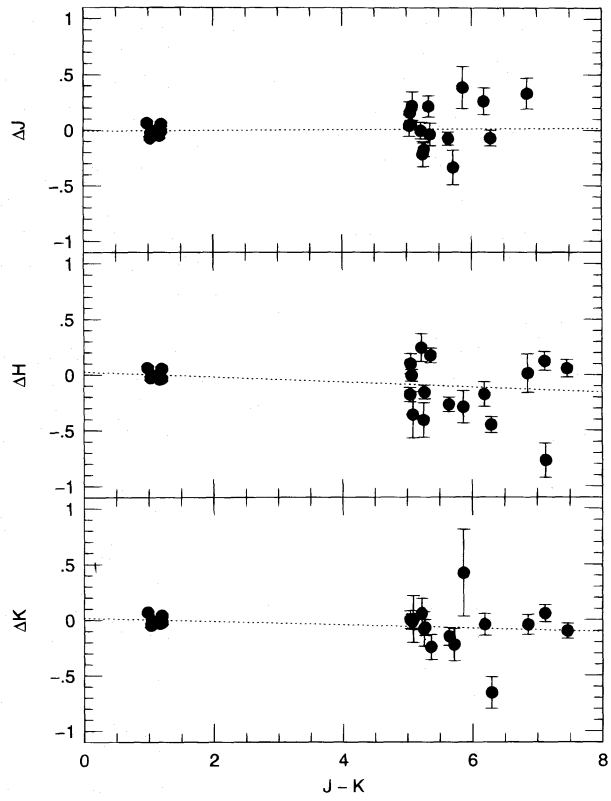

FIG. 2.—Comparison of OSIRIS and CTIO/CIT photometry. The dashed lines are weighted fits to the data. This comparison of the brightest and reddest stars in common between the OSIRIS frames and the GC photometry derived from the images of DS91 suggests no statistically significant color correction is warranted (but see text for a discussion on the flux calibration of DS91 using IRS 7). The bluest stars are giants of known magnitude in BW.

tistically significant color transformation between CTIO/CIT and OSIRIS. However, DS91 flux calibrated their data using IRS 7 which we have now found to be variable (see below). For all stars matched at any of J, H, or K, we find mean differences ΔJ, ΔH, and ΔK of 0.06 ± 0.21, -0.09 ± 0.23, and -0.05 ± 0.18 mag, respectively, when we compare Galactic center stars between DS91 and OSIRIS and exclude suspected variable stars. The good agreement between the two sets of Galactic center photometry suggests that the magnitudes assumed by DS91 for IRS 7 (from Becklin et al. 1978) were correct at the times of their observations, although we cannot rule out the possibility that there is in fact a color term between the OSIRIS and DS91 photometry and that IRS 7 varied in such a way as to mask this color term. A photometry list of bright GC sources ($K \leq 10.5$), stars with IRS numbers, and/or sources for which we have obtained 2 μm spectra (Paper II) is given in Table 1. We have included data from the DS91 images including their L-band ($\lambda \approx 3.45$ μm) measurements.

To summarize, we have derived J, H, and K magnitudes for stars in the central 2′ of the Galaxy. The overall comparison to DS91, for which we have the most stars in common of any data set at K, is good (rms difference of 0.18 mag for ~ 50 stars in the most crowded central $\sim 15''$ region). The comparison of a smaller set of stars with measured J, H, and K from the DS91 images and J, H, and K from the OSIRIS images suggests that no significant color transformation exists between the CTIO/CIT system (DS91) and the OSIRIS system (Fig. 2).

We have also compared our photometry to recent values in the literature (see the Appendix for details). The OSIRIS data are in agreement with the high angular resolution lunar occultation measurements of Simon et al. (1990) and Simons, Hodapp, & Becklin (1990) and consistent with the single-source PSF fitting of Tollestrup, Capps, & Becklin (1989). OSIRIS K magnitudes are systematically faint compared to the aperture photometry of Rieke, Rieke, & Paul (1989) and Tamura et al. (1996) and the high angular resolution deconvolved images of Eckart et al. (1993, 1995) as reported by Krabbe et al. (1995). With the exception of the data of Krabbe et al. (1995), these results are consistent with the type of photometry used in each case, i.e., our crowded field photometry is in agreement with the very high resolution lunar occultation results and is systematically fainter than the previous aperture photometry. Our results are conservative in the sense that they are generally *fainter* than previous photometry, and we will use them to show that a component of *brighter* stars exists in the GC relative to BW.

2.2. *Variability of IRS 7 and Other Stars*

Our photometry shows that IRS 7 has varied in brightness at J, H, and K by approximately 0.8, 0.5, and 0.3 mag, respectively. We also confirm the variability of IRS 9 and 12N found at K by Tamura et al. (1996) by finding ΔJ of approximately 1.0 and 1.7 mag for IRS 9 and 12N, respectively, compared to previous photometry.

Table 2 details the photometry of IRS 7 for our primary and secondary images. These data show that IRS 7 was brighter in 1993 July at J and K than previously (Becklin et al. 1978). Both of the primary H and K measurements were saturated for IRS 7 on our frames. However, analysis of the two narrow-band images (near 2.2 μm) and secondary H and K images shows that IRS 7 was also brighter at these wavelengths relative to Becklin et al. (1978). The IRS 7 J magnitude derived from the 1995 April 24 images taken at Lowell Observatory was consistent with its former value (13.8, Table 1). The photometry of DS91 taken in 1989 September and 1990 April provides another data point for IRS 7. DS91 used IRS 7 to calibrate their images, and since our comparison of the OSIRIS photometry with DS91 (Fig. 2) is consistent with no color transformation relative to the CTIO/CIT system, it seems likely that IRS 7 had the same near-infrared magnitudes at the time of the DS91 and Becklin et al. (1978) observations. Tamura et al. (1994, 1996) reported evidence that the K mag of IRS 7 may have brightened by ~ 0.15 mag from 1991 to 1992 but found no brightening when comparing data from 1991 and 1993. We have not added the Tamura et al. data to Table 2 because it is tied only to aperture photometry relative to IRS 1W, with no local sky subtraction.

IRS 9 and IRS 12N were brighter at J compared to DS91 (Table 2). These stars were found to be variable by Tamura et al. (1994, 1996), so they, like IRS 7, were not included in the color correction analysis discussed above. Tamura et al. (1996) report a steady brightening of both IRS 9 and 12N from 1991 July to 1993 August. We find the H and K magnitudes for these two stars to agree between DS91 (1989 September) and OSIRIS (1993 July) but find that J brightens between DS91 (1990 April) and OSIRIS (1993 July), as given in Tables 1 and 2. It appears that IRS 9 and IRS 12N both became fainter sometime between 1989 September and

TABLE 2

VARIABLE STARS IN THE GALACTIC CENTER

Name	J	H	K	Date	Data Set	Filters[a]
IRS 7	13.8 ± 0.1	9.3 ± 0.10	6.7 ± 0.1	1975 Jun/Jul	Becklin et al. 1978	*J, H, K*
IRS 7	...	9.3 ± 0.10	6.7 ± 0.1	1989 Sep	DS91[b]	*H, K*
IRS 7	13.8 ± 0.1	...	...	1990 Apr	DS91[b]	*J*
IRS 7	...	8.82 ± 0.10	6.40 ± 0.10	1993 May	OSIRIS/Lowell	*H, KND*
IRS 7	13.04 ± 0.04	...	6.43 ± 0.04	1993 Jul	OSIRIS/CTIO	*J, NBK*
IRS 7	13.88 ± 0.05	...	...	1995 Apr	OSIRIS/Lowell	*J*
IRS 9	...	10.85 ± 0.04	8.61 ± 0.03	1989 Sep	DS91	*H, K*
IRS 9	15.94 ± 0.06	...	...	1990 Apr	DS91	*J*
IRS 9	14.98 ± 0.03	10.99 ± 0.04	8.53 ± 0.04	1993 Jul	OSIRIS/CTIO	*J, H, NBK*
IRS 12N.....	...	11.36 ± 0.03	8.48 ± 0.05	1989 Sep	DS91	*H, K*
IRS 12N.....	17.16 ± 0.22	...	...	1990 Apr	DS91	*J*
IRS 12N.....	15.53 ± 0.03	11.41 ± 0.04	8.58 ± 0.04	1993 Jul	OSIRIS/CTIO	*J, H, NBK*

[a] Filters used to derive J, H, and K magnitudes. J, H, and K are broad-band filters. *KND* is broad-band K with a 1% neutral density filter. *NBK* is K magnitude derived from two narrow-band filters ($\Delta\lambda/\lambda = 1\%$) near 2.2 μm; see text.

[b] DS91 photometry is consistent with J, H, and K magnitudes of IRS 7 being the same as for Becklin et al. 1978; see text.

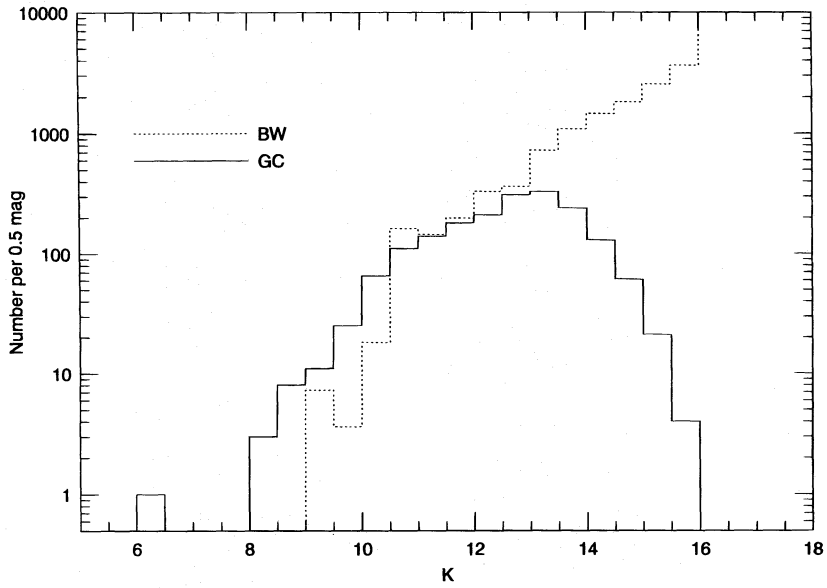

FIG. 3.—The observed K-band (2.2 μm) luminosity function (*solid histogram*) and BW luminosity function (*dotted histogram*). The BW relation has been shifted by applying a mean extinction of $A_K = 3.5$. The two luminosity functions were combined at $K = 11.5$ to create an artificial luminosity function for use in estimating the completeness limit of the K-band data. The BW component was normalized so that it joined smoothly with the observed luminosity function. See the discussion in the text and Fig. 4.

1990 April, followed by a steady increase in brightness until they had returned to their 1989 September brightnesses by 1993 July.

Table 1 shows both DS91 and OSIRIS photometry. Twelve stars with K measured from both data sets have $\Delta K > 0.2$. Of these, four stars have $\Delta K > 3\ \sigma$ and, thus, may have varied between the time in which the DS91 and OSIRIS data were taken (IRS 1NE, 6E, 21, and star 87 = IRS A19 for Tamura et al. 1996). Note also that $H-K$ and $J-L$ are the only DS91 colors which are unaffected by possible variability.

2.3. *Artificial Star Experiments*

Tests were conducted using artificial stars to assess our completeness limits and effects of crowding on the H and K frames. Because the GC is extremely crowded, complete artificial frames were constructed rather than adding stars to the original data. For the purpose of determining an estimate of the completion limit at K, a luminosity function was constructed as the sum of two components: the observed luminosity function for the bright stars and a renormalized BW luminosity function (Tiede, Frogel, & Terndrup 1995) for fainter stars ($9 \leq K_0 \leq 15.0$) with a mean reddening of $A_K = 3.5$ mag (see below) added. Hereafter, magnitudes and colors with a "0" subscript will refer to intrinsic, or dereddened values. The observed luminosity function and the BW relation are shown in Figure 3. The BW component was added to the observed luminosity function such that it joined smoothly with the observed luminosity function at $K = 11.5$. This composite function was

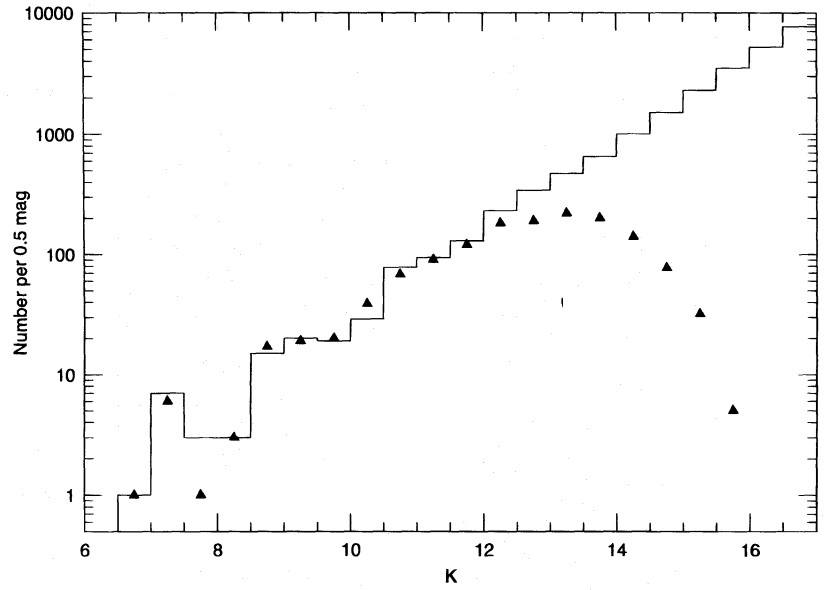

FIG. 4.—The artificial K-band (2.2 μm) luminosity function (*solid histogram*) created by combining the observed GC luminosity function for $K < 11.5$ and the BW LF (Tiede et al. 1995), reddened by $A_K = 3.5$, for $K > 11.5$. The two luminosity functions in Fig. 3 were combined and then fitted by a power law. The power law was randomly sampled to produce the artificial luminosity function shown here. The recovered histogram (*solid triangles*) suggests the GC K-band data is complete to $K \lesssim 12$.

then approximated by a smooth power-law distribution [$\log(N) = 0.35 \times K + \text{const.}$]. The power-law luminosity function and an assumed radial surface density distribution ($\Sigma \sim R^{-0.8}$, core radius of 4″; Becklin & Neugebauer 1968; Eckart et al. 1993, 1995) were sampled randomly to distribute stars on the artificial frame. Execution of DAOPHOT in an analogous manner to that of the original frames suggests that the GC K frames are complete to $K \lesssim 12$. The completeness limit may be less than this since the bright end of the test luminosity function was taken from the observed luminosity function. The input (power-law) luminosity function and the recovered one are shown in Figure 4. A similar test was made at H and suggests the H-band images are complete to $\lesssim 14.25$.

To assess the affect of image crowding on the bright end of the observed luminosity function, 10 frames were constructed as above but using only the reddened BW luminosity function. We added long-period variables (LPVs) to the Tiede et al. (1995) relation according to the numbers added by spectral type given in FW87 (10 stars). The BW luminosity function was normalized to have the same observed luminosity as one of the GC frames, $L_K = 0.95 \times 10^6\ L_{\odot K}$ ($R_0 = 8$ kpc and $A_K = 3.5$, see below). This value of the observed K-band luminosity corresponds to an observed flux that is within 10% of that reported by Becklin & Neugebauer (1968) for their 1.″8 diameter beam measurement, accounting for the slightly larger OSIRIS frame area. The BW relation was then fitted by a smooth combination of third-order splines to generate the actual input artificial luminosity functions. This fitting process resulted in input luminosity functions with $9.9 \leq K \leq 18.4$. A total of 80,300 stars were distributed on each frame with an average of 227 stars per frame at $K \leq 10.9$. For the 10 frames, 7.1 stars, on average, were extracted with magnitudes brighter than any star in the input luminosity function. On average, 0.5 stars were up to 0.75 mag brighter than the brightest star in the input luminosity function per frame, one star was up to 0.5 mag brighter per frame, and 5.6 stars were <0.25 mag brighter. It is clear that we should expect a small number of stars in our real frames to have similar overestimates of their brightnesses. However, the number of such stars is small and suggests that we have not overestimated the K magnitudes for a significant number of the brightest GC stars due to chance alignments of bright stars.

3. DISCUSSION

3.1. *The Color-Magnitude Diagram*

The GC color-magnitude diagrams (CMDs) are shown in Figure 5. These diagrams clearly show the effects of strong and variable interstellar extinction. The paucity of stars to the lower right in each panel of Figure 5 graphically demonstrates the sensitivity of the observations to increased reddening: it is difficult to detect faint, red stars at progressively shorter wavelengths. Differential reddening results in much larger color differences than the intrinsic color differences between hot and cool stars in the observed Galactic center CMD, so that these populations cannot be separated purely by the observed photometry. This is shown in Figure 5 where we have overplotted the CMD of the old stellar population from BW (FW87) with values of $A_K = 2$ mag and $A_K = 4$ mag, respectively. Except for the bright M supergiant, IRS 7, the majority of the GC CMDs are consistent with the CMD of the BW population. The differences between the GC and BW become more apparent only when the dereddened K-band luminosity function (see below) or spectra of individual stars are considered (Paper II).

Figure 5 also shows the positions of hot and cool stars with spectral identifications. Most hot stars appear more to the blue in $H-K$ and (particularly) $J-K$. This suggests, as expected, that part of the dispersion in the observed CMDs is due to the mixed young and old populations. Note that several possible hot stars such as IRS 1W and IRS 6E with extremely red continua (Rieke et al. 1989; Libonate et al. 1995; Blum et al. 1995a; Krabbe et al. 1995) are among the reddest stars in the CMD. Identifications for individual sources from spectra are given in Table 1.

3.2. *Extinction and the Color-Color Diagram*

The $J-H$ versus $H-K$ color-color diagram, Figure 6, allows us to estimate the interstellar extinction to individual stars. Plotted along with the approximately 450 stars in Figure 6 is the interstellar reddening line based upon the interstellar extinction curve of Mathis (1990) for which $E(J-H)/E(H-K) \sim 1.6$. The majority of stars in the GC field lie along this relation at positions corresponding to substantial A_K, suggesting they are stars of normal colors seen through varying amounts of interstellar extinction. For intrinsic $J-H$ and $H-K$ of 0.7 and 0.3 mag (corresponding to late-type M giants; FW87), the majority of stars in Figure 6 lie at 2 mag $\lesssim A_K \lesssim$ 4 mag.

The intrinsic $J-H$ and $H-K$ colors of normal stars span a relatively small range in magnitude (see, e.g., Frogel et al. 1978 and FW87). For large values of extinction, as indicated by Figure 6, relatively accurate estimates of A_K can be made by assuming a single pair of intrinsic colors. We have calculated A_K for the stars in Figure 6 which have $H-K$ within ± 0.5 mag of the reddening line (375 stars) by adopting intrinsic $J-H$ and $H-K$ of 0.7 and 0.3 mag and using the Mathis (1990) interstellar extinction law. Here, we take an average of A_K as determined from the two colors. The mean A_K for stars with extinction determined in this way is 2.82 ± 0.71 mag. For stars detected only at H and K (approximately 700 stars), A_K was determined by dereddening the star to an assumed intrinsic BW giant $H-K$ from FW87. The mean A_K for stars with extinction determined in this way is 3.58 ± 0.79 mag.

For stars detected only at K (approximately 800), other techniques must be used to estimate A_K. Figure 7 shows the *observed* luminosity function at K separately for stars detected at J, H, and K; for stars detected at H and K; and for stars detected only at K. These three histograms are progressively shifted to fainter K as would be expected for stars intrinsically fainter at the same A_K. However, there is also large overlap between the histograms. This would be expected for stars of the same apparent K brightness that are seen through larger A_K. This effect was already demonstrated by the different values of mean A_K determined for the stars with J, H, and K ($A_K = 2.8$ mag) versus those with A_K derived only from H and K ($A_K = 3.6$ mag). The effect is also immediately apparent in the middle panels of Figure 5. If the brightest stars detected only at K (Fig. 7 [*solid histogram*]) have typical intrinsic colors, then a lower limit for A_K can be estimated by assuming an H magnitude equal to the completeness limit (14.25). Stars detected only at K must have $A_K > 3.6$ mag for $K < 11.6$ mag to avoid detection at H. In this case, stars detected only at K would have

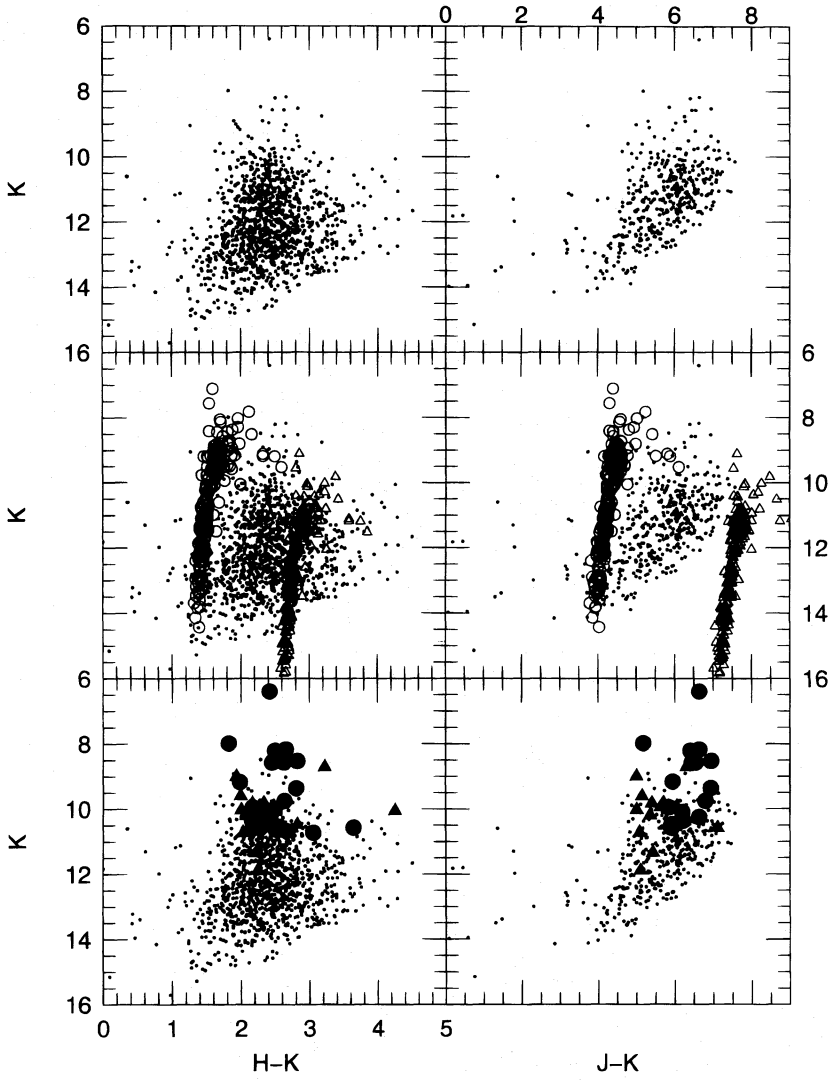

FIG. 5.—Observed color-magnitude diagrams for the $\sim 2' \times 2'$ field of the Galactic center. The three pairs of plots show the same observed Galactic center photometry (*small filled circles*) with different overlays. The very red colors and large dispersion in $J-K$ and $H-K$ (*top two panels*) demonstrate the strong and variable interstellar extinction toward the Galactic center. The importance of obtaining spectra is demonstrated by the fact that based solely on observed magnitudes and colors, all but one of the Galactic center stars in the CMD is consistent with an old stellar population like that in Baade's window (*middle two panels*), after interstellar extinction values of $A_K = 2$ mag (*open circles*) and $A_K = 4$ mag (*open triangles*) are applied to the Baade's window data to match the estimated extinction toward the Galactic center. Data for Baade's window were taken from Frogel & Whitford (1987). Galactic center stars with spectral classifications (*bottom two panels*) from near-infrared spectra are identified as either hot (*large filled triangles*) or cool (*large filled circles*) stars.

A_K of 6.5 mag for $K = 9.25$ mag, 5.9 mag for $K = 9.75$ mag, 5.3 mag for $K = 10.25$ mag, 4.6 mag for $K = 10.75$ mag, and 4.0 mag for $K = 11.25$ mag. For the stars detected only at K, therefore, a lower limit of $A_K = 3.6$ mag or the value of A_K derived by assuming an $H-K$ using the H-band limiting magnitude, whichever was greater, was adopted.

For the stars in Table 1 with L-band magnitudes from the DS91 images, A_K was computed from the same reddening law and an assumed intrinsic $K-L$ of 0.2 mag (Johnson 1966). If $K-L$ was within ± 0.5 mag of the reddening line for $H-K$ versus $K-L$ and no excess was indicated by the $J-H$ and $H-K$ colors, this value was averaged with the other determinations (eight stars). The average A_K determined from the $K-L$ color (25 stars, including stars with only K and L) is 4.0 ± 2.0 mag. This value is affected strongly by the stars IRS 2L, 3, 10EL, and 21 that had only $K-L$ measured. All are extremely red and may have much larger intrinsic colors (e.g., due to circumstellar dust emission) and hence smaller interstellar reddening. If these four are excluded, the average A_K determined from $K-L$ would be 3.3 ± 1.0 mag.

These individually derived reddening values were used in constructing the dereddened K-band luminosity function for the GC (see below); results for all stars with $K \leq 10.5$ mag, stars with IRS numbers, and stars for which K-band spectra are available (Paper II) in Table 1. The mean value of A_K for all stars with one or more observed near-infrared colors is 3.3 ± 0.9 mag.

3.3. *Stars with Infrared Excesses*

The color-color diagram (Fig. 6) is also useful in identifying stars with potential excess emission. Stars falling to the right of the reddening line by more than 0.5 mag in $H-K$ are candidates for objects with excess emission. This difference in $H-K$ from the reddening line is approximately 3 times the difference between the reddest mean M giant $(H-K)_0$ in FW87 and the value we adopted for use in dereddening the photometry. A_K was determined from $J-H$ only

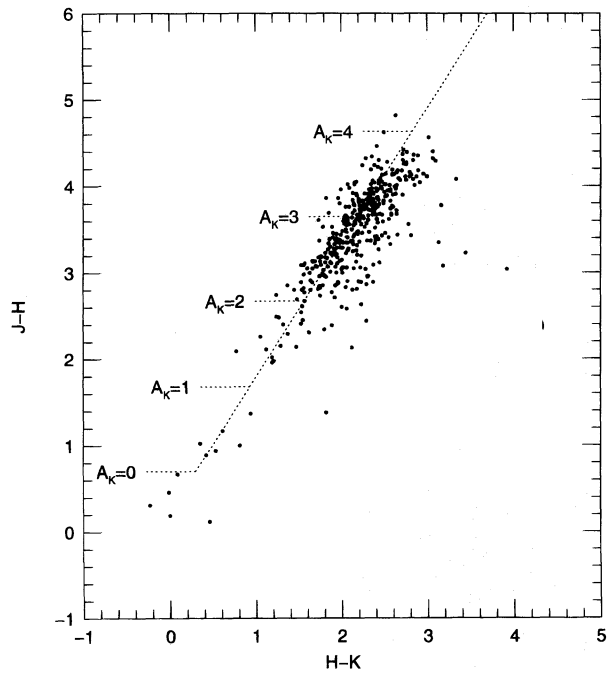

FIG. 6.—$J-H$ vs. $H-K$ color-color diagram. The dashed line represents the interstellar extinction law of Mathis (1990) for which $E(J-H)/E(H-K) \sim 1.6$. Stars that fall to the right of the reddening line by more than 0.5 mag in $H-K$ may have intrinsic excess; see text.

for these stars. IRS 1W is a good example of this class: it stands well off the reddening line in Figure 6 with an apparent infrared "excess" and has a 2 μm spectrum thath is extremely red (Blum et al. 1995a).

Becklin (1995) and Krabbe et al. (1995) have suggested that GC sources with red, featureless 2 μm spectra and colors suggesting an infrared excess are possibly young stellar objects (YSOs), each still embedded in its dusty cocoon and/or having an accretion disk that provides a significant infrared excess. IRS 1W is one example of a candidate YSO; another is IRS 21, which has a spectrum similar to IRS 1W (Krabbe et al. 1995). IRS 21 is barely visible on our J and H images but is too faint to be confidently extracted, in part because of its proximity to other bright stars. We place lower limits of $J > 17.6$ mag and $H > 14.7$ mag on IRS 21, based on 1 pixel radius aperture photometry relative to nearby IRS 33 (which may have similar background). This implies $H-K > 4.3$ mag for IRS 21.

We have summarized published observations of some luminous and well-studied YSOs in Table 3 in order to compare YSOs to the *observed* magnitudes and colors of YSO candidates in the GC (Table 1). This comparison requires correcting the YSO magnitudes to a distance of 8 kpc, adding the foreground extinction toward the GC ($A_K = 3.6$ mag) and also subtracting any foreground extinction from the molecular cloud surrounding the YSO. It is difficult to correct YSOs for foreground extinction because the intrinsic colors of YSOs are uncertain and very model dependent (Shu, Adams, & Lizano 1987). We have therefore made two extreme assumptions about the intrinsic colors of YSOs: that either all of the observed $H-K$ color of the YSO is intrinsic to the source (red YSO) or all of the observed $H-K$ color of the YSO is due to foreground extinction (blue YSO).

The K magnitudes and $H-K$ colors of IRS 1W and IRS 21, and other GC sources with IR excesses, are well matched by luminous YSOs if the $H-K$ colors of these YSOs are partially intrinsic and partially due to foreground reddening. If YSOs are intrinsically red, with their observed $H-K$ color equal to their intrinsic $H-K$ color, then they would be too faint and in many cases too red to account for the red, luminous GC stars. If YSOs are intrinsically blue, with their observed $H-K$ color entirely due to foreground reddening, then they can easily account for the observed magnitudes of red, luminous GC sources with featureless spectra such as IRS 1W and IRS 21, but their $H-K$ color

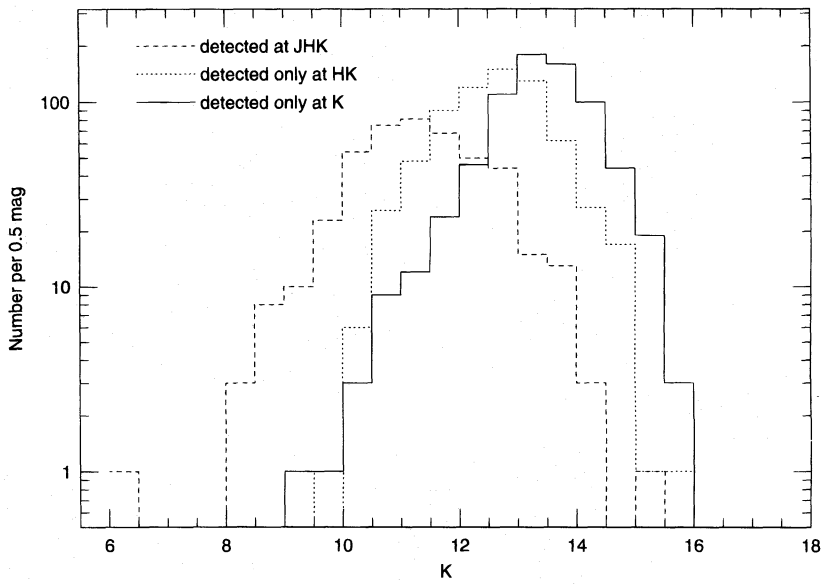

FIG. 7.—Observed K-band luminosity function for stars detected at J, H, and K (*dashed histogram*), for stars detected only at H and K (*dotted histogram*), and for stars detected only at K (*solid histogram*). Stars detected at J, H, and K have mean A_K (2.8 $\pm$ 0.7) smaller than that of those detected only at H and K (3.6 $\pm$ 0.8). Similarly, some stars detected only at K are probably intrinsically luminous stars that are more heavily reddened (A_K up to 6.5) than the mean value for those detected at $H-K$; see discussion in text.

TABLE 3

YOUNG STELLAR OBJECT (YSO) PHOTOMETRY

YSO NAME	OBSERVED (Observed YSO at 8 kpc)[a]		REDDENED (Red YSO + GC Extinction)[b]		REDDENED (Blue YSO + GC Extinction)[c]		REFERENCES
	K	$H-K$	K	$H-K$	K	$H-K$	
CRL 2591	8.6	3.7	12.2	6.0	6.3	2.3	1
CRL 2059	8.7	2.6	12.3	4.9	8.2	2.3	2
CRL 490	9.8	2.6	13.4	4.9	9.3	2.3	1
CRL 989	9.9	2.6	13.5	4.9	9.4	2.3	3
W33A	10.6	2.7	14.2	5.0	9.9	2.3	4
S140/IRS 1	10.7	2.4	14.3	4.7	10.5	2.3	5
CRL 961	10.8	1.7	14.4	4.0	11.7	2.3	6
NGC 7538/IRS 9	10.9	5.8	14.5	8.1	5.3	2.3	7
Mon R2/IRS 3	11.2	3.0	14.8	5.3	10.0	2.3	8
BN	11.2	4.6	14.8	6.9	7.5	2.3	9
S255/IRS 1	11.6	2.2	15.2	4.5	11.7	2.3	10

[a] Observed K magnitude, corrected to a GC distance of 8 kpc, and observed $H-K$ color of YSO. No correction has been applied for either the reddening of the YSO or the extinction toward the GC.

[b] Predicted K magnitude and $H-K$ color of YSO at the GC, if the YSO is intrinsically red. This assumes the intrinsic $H-K$ color of the YSO equals its observed $H-K$ color, and there is no correction to the YSO for extinction in its surrounding molecular cloud. An average GC extinction of $A_K = 3.6$ mag and $E(H-K) = 2.3$ mag has been applied.

[c] Predicted K magnitude and $H-K$ color of YSO at the GC, if the YSO is intrinsically blue. This assumes the intrinsic color of the YSO is $H-K = 0.0$ and the observed $H-K$ color of the YSO is used to correct for extinction in its surrounding molecular cloud. An average GC extinction of $A_K = 3.6$ mag and $E(H-K) = 2.3$ mag has been applied.

REFERENCES FOR H AND K PHOTOMETRY.—(1) Merrill & Stein 1976; (2) Simon et al. 1985; (3) Allen 1972; (4) Chini, Krugel, & Wargau 1987; (5) Evans et al. 1989; (6) Castelaz et al. 1985; (7) Werner et al. 1979; (8) Beckwith et al. 1976; (9) Becklin & Neugebauer 1967; (10) Evans, Blair, & Beckwith 1977. We adopted published photometry which was obtained with a beam most closely matching the 0.04 pc spatial resolution of our GC images. CRL 961E and CRL 961W are separated by 0.03 pc; flux from both components is included for CRL 961. Distances for all sources are from Wynn-Williams 1982.

would be too blue. The truth probably lies someplace in between these extremes: some of the YSO color is intrinsic and some is due to reddening, which makes it plausible that YSO colors and magnitudes can match those of red, luminous sources in the GC.

IRS 6E, another red object, would have $(H-K)_0 = 2.3$ mag if a typical value of A_K (3.6 mag) is assumed. This star has been identified as a late-type WR star (WC9) by Krabbe et al. (1995). The weak emission lines detected by Krabbe et al. for IRS 6E (relative to WC9 stars in the field) are consistent with a large excess. WC8–9 stars have been identified in the field with large excesses because of circumstellar dust emission. Such stars may have weak or no infrared emission lines as a consequence (Cohen et al. 1991). JHK photometry for dusty WCL stars (Williams, van der Hucht, & Thé 1987; Cohen et al. 1991) and V and R photometry to estimate A_V (and hence A_K) suggest that these stars have $(J-H)_0 = 0.76$ mag to 1.8 mag and $(H-K)_0 = 0.90$ mag to 1.60 mag. If IRS 6E has $(H-K)_0 = 1.6$ mag, A_K would be 4.2 mag using the observed $H-K$. The photometry of Williams et al. (1987) also suggests that WC9 stars may have $(H-K)_0$ as small as 0.3 mag; therefore, for consistency, we have not adopted a different color for IRS 6E in Table 4 than any other star even though its photometry and spectrum suggest it may be intrinsically more red. Other WC9 stars identified in the GC (Blum et al. 1995a; Krabbe et al. 1995) also show weaker emission lines than field WR stars. These have smaller (yet nonzero) $(H-K)_0$ (see Table 4), so it is not clear what may cause the observed dilution in these cases (source crowding is a possibility).

3.4. *The K-Band Luminosity Function*

Using the results of DAOPHOT crowded field photometry and the extinction estimates above, we have constructed the dereddened K-band luminosity function (KLF) for the inner $\sim 2'$ of the Galaxy (Fig. 8). As discussed in § 2.3, because of extreme crowding at our spatial resolution (FWHM $\lesssim 1''$), the luminosity function is complete only to $K_0 \lesssim 8.5$ mag. Only stars with $A_K > 2$ mag were included in the KLF in an attempt to eliminate foreground stars (40 stars of 1100 with measured A_K had $A_K < 2$ mag). OSIRIS data were used in the KLF for stars whose DS91 K magnitude differed by more than 0.2 mag from the OSIRIS K magnitude (approximately 15 stars; see § 2.1).

In Figure 8, we compare the KLF to a renormalized KLF for the old stellar population in BW (FW87; Tiede et al. 1995). The BW relation has been renormalized by requiring that it account for the observed K luminosity in the GC. For our K images (adding up the total observed flux on an image), this corresponds to $L_K \approx 2.0 \times 10^7\ L_{\odot K}$ assuming a mean A_K of 3.3 mag (this is an average A_K for all stars for which we calculated A_K from one or more observed near-infrared colors) and $R_0 = 8$ kpc. This includes a few percent correction that sets the darkest region of the sky-subtracted images to zero flux. An alternate normalization scheme gives a similar result: assuming all the dynamically inferred mass in the GC (Genzel, Hollenbach, & Townes 1994, but corrected for the projected mass within our $\sim 2'$ field and taking $R_0 = 8$ kpc) is in a BW-like population with $M/L = 1.2\ M_\odot/L_{\odot K}$ (Genzel et al. 1994) suggests $L_K \approx 2.3 \times 10^7\ L_{\odot K}$.

The comparison of the GC KLF and the renormalized BW KLF (Fig. 8) shows an excess of bright stars at $K_0 \lesssim 7$ mag that are presumably due to more recent star formation epochs. The renormalized BW KLF has stars as bright as $K_0 = 5.5$ mag while the GC KLF extends to $K_0 \approx 2.0$ mag. The BW KLF has about 30 stars brighter than $K_0 = 7.0$ mag; the GC KLF has 149 stars in this range. The artificial star experiments described in § 2.3 suggest roughly 3% of the brightest stars in simulated GC images might have

TABLE 4

GALACTIC CENTER REDDENING-CORRECTED PHOTOMETRY

ID	Name	K_0[a]	A_K[b]	$(J-K)_0$[a]	$(H-K)_0$[a]	$(K-L)_0$[a]	Notes
1.....		4.78 ± 0.08	5.62	...	...	...	[c]
2.....		4.44 ± 0.05	5.83	...	...	...	[c]
3.....		4.00 ± 0.05	6.10	...	...	...	[c]
4.....		6.70 ± 0.08	3.67 ± 0.06	0.93 ± 0.12	0.43 ± 0.07	...	
5.....		6.74 ± 0.06	3.51 ± 0.05	0.94 ± 0.10	0.41 ± 0.06	...	
6.....		2.88 ± 0.03	6.79	...	...	...	[c]
7.....		5.97 ± 0.06	3.83 ± 0.05	0.97 ± 0.10	0.35 ± 0.06	...	
8.....		6.73 ± 0.08	3.50 ± 0.06	1.00 ± 0.12	0.30 ± 0.08	...	
9.....		6.63 ± 0.06	3.29 ± 0.05	0.98 ± 0.09	0.34 ± 0.06	...	
10.....		6.97 ± 0.10	3.47 ± 0.10	1.51 ± 0.18	0.81 ± 0.08	...	
11.....		1.73 ± 0.14	7.49	...	...	...	[c]
12.....		7.65 ± 0.13	2.67 ± 0.10	1.02 ± 0.19	0.26 ± 0.13	...	
13.....		6.62 ± 0.08	3.44 ± 0.07	1.86 ± 0.13	1.16 ± 0.06	...	
14.....		6.88 ± 0.06	3.60 ± 0.05	0.94 ± 0.09	0.41 ± 0.06	...	
15.....		7.16 ± 0.06	3.28 ± 0.05	0.97 ± 0.09	0.36 ± 0.06	...	
16.....		7.27 ± 0.05	2.32 ± 0.04	1.04 ± 0.08	0.23 ± 0.05	...	
17.....		6.55 ± 0.06	3.20 ± 0.05	0.91 ± 0.09	0.46 ± 0.06	...	
18.....		5.83 ± 0.09	4.36 ± 0.09	...	0.42 ± 0.08	...	
19.....		6.03 ± 0.09	4.11 ± 0.09	0.94 ± 0.20	0.42 ± 0.08	...	
20.....		7.05 ± 0.09	3.44 ± 0.08	...	0.35 ± 0.07	...	
21.....		7.11 ± 0.05	3.13 ± 0.05	1.02 ± 0.09	0.26 ± 0.05	...	
22.....	BSD WC9	7.89 ± 0.11	2.83 ± 0.10	...	0.30 ± 0.09	...	
23.....		6.56 ± 0.05	3.18 ± 0.04	1.00 ± 0.08	0.30 ± 0.05	...	
24.....		7.38 ± 0.06	2.80 ± 0.05	1.01 ± 0.10	0.28 ± 0.06	...	
25.....	AF NWB	9.41 ± 0.13	2.22 ± 0.10	1.63 ± 0.19	0.93 ± 0.14	...	
26.....	BSD WC9B	9.64 ± 0.25	2.42 ± 0.23	...	0.30 ± 0.21	...	
27.....		5.49 ± 0.09	3.53 ± 0.09	...	0.44 ± 0.08	...	
28.....	IRS 11	6.18 ± 0.09	3.00 ± 0.06	1.11 ± 0.13	0.10 ± 0.09	...	
29.....	AF NW	9.69 ± 0.15	2.20 ± 0.11	1.56 ± 0.22	0.86 ± 0.16	...	
30.....	IRS 6WB	7.65 ± 0.42	3.86	...	...	...	[c]
31.....	IRS 6W	7.23 ± 0.10	3.01 ± 0.07	0.90 ± 0.14	0.48 ± 0.10	...	
32.....	AF B	8.61 ± 0.11	2.63 ± 0.08	1.00 ± 0.15	0.29 ± 0.10	...	
33.....	AF	8.14 ± 0.08	2.58 ± 0.06	0.94 ± 0.11	0.41 ± 0.07	...	
34.....		7.01 ± 0.13	3.18 ± 0.11	...	0.36 ± 0.10	...	
35.....	IRS 30	6.93 ± 0.13	3.65 ± 0.13	1.12 ± 0.26	0.09 ± 0.13	−0.78 ± 0.24	DS91 *JH*
36.....		7.80 ± 0.06	2.57 ± 0.04	1.04 ± 0.08	0.23 ± 0.06	...	
37.....	IRS 30B	6.72 ± 0.16	4.44	...	...	...	[c]
38.....	IRS 6E	3.77 ± 0.28	6.28 ± 0.28	...	0.30 ± 0.25	...	
38.....	IRS 6E	4.63 ± 0.15	5.16 ± 0.14	...	...	0.20 ± 0.11	
39.....		7.14 ± 0.06	3.23 ± 0.05	0.98 ± 0.09	0.33 ± 0.06	...	
40.....		3.97 ± 0.05	6.12	...	...	...	[c]
41.....		6.92 ± 0.19	3.22 ± 0.16	...	0.36 ± 0.14	...	
42.....	IRS 13W	6.22 ± 0.12	4.74	...	...	...	[c]
42.....	IRS 13W	5.62 ± 0.38	4.99 ± 0.37	...	...	0.20 ± 0.28	
43.....		6.89 ± 0.06	3.18 ± 0.05	1.01 ± 0.09	0.29 ± 0.06	...	
44.....	IRS 12NB	7.49 ± 0.13	2.61 ± 0.08	1.48 ± 0.17	0.78 ± 0.13	...	
45.....	IRS 2	5.26 ± 0.21	5.31 ± 0.20	...	0.30 ± 0.18	...	
45.....	IRS 2	6.43 ± 0.28	3.90 ± 0.26	...	...	0.20 ± 0.20	
46.....	IRS 34	5.68 ± 0.07	5.07	...	...	...	[c]
46.....	IRS 34	7.36 ± 0.36	3.12 ± 0.35	...	...	0.20 ± 0.27	
47.....	IRS 12S	6.95 ± 0.07	3.00 ± 0.06	1.01 ± 0.11	0.29 ± 0.07	...	
48.....	IRS 22	5.43 ± 0.06	2.52 ± 0.05	1.10 ± 0.06	0.24 ± 0.07	...	
49.....	IRS 2L	3.87 ± 0.45	7.81 ± 0.40	...	...	0.20 ± 0.30	
50.....	IRS 12N	4.74 ± 0.14	3.79 ± 0.14	0.90 ± 0.23	0.49 ± 0.11	−1.21 ± 0.19	
51.....		4.09 ± 0.20	6.04	...	...	...	[c]
52.....	IRS 13E	6.85 ± 0.18	2.97 ± 0.12	0.91 ± 0.24	0.46 ± 0.16	...	
52.....	IRS 13E	3.97 ± 0.33	5.63 ± 0.30	...	...	0.20 ± 0.10	
53.....	IRS 3	6.72 ± 0.11	4.43	...	...	...	[c]
53.....	IRS 3	0.84 ± 0.16	9.94 ± 0.14	...	...	0.20 ± 0.11	
54.....	IRS A7	7.27 ± 0.08	3.23 ± 0.06	0.96 ± 0.12	0.38 ± 0.08	−0.83 ± 0.22	
55.....	IRS 29S	7.87 ± 0.29	2.68 ± 0.08	1.58 ± 0.31	0.88 ± 0.29	...	
56.....	IRS 29N	5.22 ± 0.20	4.69 ± 0.18	...	...	0.20 ± 0.14	
57.....	IRS 20	7.52 ± 0.08	3.06 ± 0.06	0.97 ± 0.13	0.35 ± 0.08	−0.92 ± 0.49	
58.....		7.17 ± 0.05	3.21 ± 0.04	0.96 ± 0.09	0.37 ± 0.05	...	
59.....	MPE −1.0-3.5	8.50 ± 0.89	3.40 ± 0.86	...	...	0.20 ± 0.65	
60.....	IRS 14SW	6.59 ± 0.07	3.56 ± 0.06	0.98 ± 0.12	0.34 ± 0.07	...	
61.....	IRS 33W	7.75 ± 0.11	3.12 ± 0.09	1.04 ± 0.18	0.22 ± 0.11	−0.65 ± 0.33	
62.....	IRS 15SW	7.53 ± 0.07	2.86 ± 0.05	0.97 ± 0.10	0.35 ± 0.07	...	
63.....	IRS A11	8.02 ± 0.12	2.88 ± 0.10	0.61 ± 0.18	0.21 ± 0.10	0.44 ± 0.16	
64.....		6.69 ± 0.05	3.44 ± 0.05	0.98 ± 0.09	0.34 ± 0.06	...	
65.....	IRS 16NW	7.51 ± 0.07	2.52 ± 0.05	0.94 ± 0.10	0.42 ± 0.06	...	
66.....	IRS 7	2.92 ± 0.09	3.48 ± 0.09	1.02 ± 0.18	0.23 ± 0.11	...	

TABLE 4—*Continued*

ID	Name	K_0[a]	A_K[b]	$(J-K)_0$[a]	$(H-K)_0$[a]	$(K-L)_0$[a]	Notes
66	IRS 7	2.98 ± 0.16	3.72 ± 0.13	1.10 ± 0.25	0.25 ± 0.16	0.16 ± 0.16	
67	IRS 33E	7.01 ± 0.07	2.93 ± 0.06	0.92 ± 0.11	0.44 ± 0.07	−0.75 ± 0.25	
68	IRS 14NE	6.13 ± 0.07	3.61 ± 0.05	0.97 ± 0.10	0.36 ± 0.07	...	
69		6.03 ± 0.07	3.76 ± 0.06	0.96 ± 0.12	0.38 ± 0.06	...	
70		6.57 ± 0.09	3.32 ± 0.07	0.94 ± 0.13	0.40 ± 0.09	...	
71	IRS 16SW	7.00 ± 0.08	2.60 ± 0.06	0.96 ± 0.11	0.36 ± 0.08	...	
71	IRS 16SW	7.29 ± 0.24	2.06 ± 0.22	...	...	0.20 ± 0.17	
72		7.38 ± 0.06	1.67 ± 0.04	1.05 ± 0.09	0.21 ± 0.06	...	
73		7.31 ± 0.11	2.72 ± 0.08	1.02 ± 0.16	0.34 ± 0.10	0.18 ± 0.12	
74	IRS 16C	7.26 ± 0.07	2.56 ± 0.06	1.27 ± 0.11	0.55 ± 0.07	−0.02 ± 0.09	
75	IRS 15NE	5.80 ± 0.06	3.16 ± 0.05	0.93 ± 0.09	0.42 ± 0.06	...	
76	OSUF 1	8.56 ± 0.13	2.80 ± 0.11	0.91 ± 0.20	0.46 ± 0.13	...	
77	MPE +1.6-6.8	6.65 ± 0.11	3.28 ± 0.08	0.76 ± 0.16	0.41 ± 0.11	0.30 ± 0.10	
78		4.99 ± 0.06	5.49	...	...	...	[c]
79		6.32 ± 0.17	3.41 ± 0.11	1.10 ± 0.22	0.13 ± 0.15	...	
80	IRS 16CC	7.41 ± 0.32	3.10 ± 0.30	...	...	0.20 ± 0.22	
80	IRS 16CC	7.48 ± 0.11	2.72 ± 0.08	0.97 ± 0.16	0.36 ± 0.10	...	
81	IRS 21	4.78 ± 0.05	5.62	...	...	...	[c]
81	IRS 21	4.50 ± 0.13	5.61 ± 0.12	...	...	0.20 ± 0.09	
82	TAM He1	8.45 ± 0.12	3.58	...	...	...	[d]
83	IRS 16NE	6.55 ± 0.06	2.45 ± 0.05	1.05 ± 0.09	0.39 ± 0.06	0.14 ± 0.06	
84		5.85 ± 0.08	4.03 ± 0.07	0.88 ± 0.14	0.52 ± 0.08	...	
85		8.48 ± 0.14	2.49 ± 0.12	1.08 ± 0.21	0.48 ± 0.12	0.10 ± 0.19	
86		8.21 ± 0.13	3.58	...	...	...	[d]
87	IRS A19	8.53 ± 0.44	3.08 ± 0.43	...	...	0.20 ± 0.33	
87	IRS A19	7.65 ± 0.14	3.53 ± 0.13	...	0.30 ± 0.12	...	
88		7.49 ± 0.34	2.54 ± 0.29	3.06 ± 0.51	2.36 ± 0.38	...	DS91 *H*
89	OSU He1	8.78 ± 0.23	3.58	...	...	...	[d]
90		7.19 ± 0.11	2.92 ± 0.08	1.10 ± 0.15	0.12 ± 0.10	...	
91	IRS 9	5.21 ± 0.07	3.36 ± 0.06	0.99 ± 0.14	0.30 ± 0.07	−0.33 ± 0.05	
92	IRS 1W	6.26 ± 0.07	2.48 ± 0.06	2.55 ± 0.10	1.80 ± 0.07	1.96 ± 0.07	
93		7.43 ± 0.18	3.23 ± 0.15	0.70 ± 0.29	0.29 ± 0.16	0.37 ± 0.21	DS91 *J*
94	IRS 10W	7.54 ± 0.09	2.70 ± 0.08	2.15 ± 0.15	1.45 ± 0.09	2.00 ± 0.07	
95		7.45 ± 0.13	3.08 ± 0.11	1.14 ± 0.21	0.53 ± 0.11	0.05 ± 0.16	DS91 *J*
96	IRS 1NE	7.89 ± 0.24	2.44 ± 0.22	...	...	0.20 ± 0.17	
96	IRS 1NE	6.52 ± 0.16	3.48 ± 0.14	...	0.30 ± 0.13	...	
97	IRS 1SE	6.78 ± 0.08	3.47 ± 0.07	1.03 ± 0.16	0.24 ± 0.07	...	
98	IRS 10EL[e]	3.18 ± 0.20	7.58 ± 0.18	...	...	0.20 ± 0.13	
99		6.35 ± 0.05	3.41 ± 0.04	1.00 ± 0.08	0.30 ± 0.05	...	
100		7.99 ± 0.11	2.38 ± 0.11	3.12 ± 0.19	2.42 ± 0.11	...	
101	IRS 10E	7.17 ± 0.09	3.19 ± 0.07	1.08 ± 0.13	0.16 ± 0.09	...	
102	IRS 28	5.62 ± 0.06	3.74 ± 0.05	0.91 ± 0.09	0.46 ± 0.06	...	
103	OSU C2	6.88 ± 0.07	3.22 ± 0.06	0.99 ± 0.11	0.32 ± 0.07	...	
104		7.41 ± 0.06	3.05 ± 0.05	1.01 ± 0.09	0.28 ± 0.06	...	
105		5.65 ± 0.05	3.26 ± 0.04	1.02 ± 0.08	0.27 ± 0.05	...	
106		7.05 ± 0.06	3.28 ± 0.05	0.98 ± 0.09	0.34 ± 0.06	...	
107		6.84 ± 0.05	3.26 ± 0.04	1.00 ± 0.08	0.29 ± 0.05	...	
108	IRS 19	4.64 ± 0.05	3.50 ± 0.04	0.98 ± 0.06	0.46 ± 0.06	...	
109	IRS 18	6.18 ± 0.05	3.32 ± 0.04	1.00 ± 0.08	0.30 ± 0.05	...	
110		6.22 ± 0.07	3.85 ± 0.05	0.88 ± 0.11	0.52 ± 0.06	...	
111		7.05 ± 0.08	3.34 ± 0.07	1.09 ± 0.15	0.13 ± 0.07	...	
112	OSU C3	6.48 ± 0.09	4.25 ± 0.09	...	0.38 ± 0.08	...	
113		6.50 ± 0.12	3.51 ± 0.11	...	0.38 ± 0.10	...	
114		5.44 ± 0.06	3.04 ± 0.04	0.95 ± 0.07	0.37 ± 0.07	...	
115		7.06 ± 0.06	3.20 ± 0.05	0.98 ± 0.09	0.34 ± 0.06	...	
116	OSU C1	7.17 ± 0.10	3.46 ± 0.10	...	0.35 ± 0.09	...	
117		7.35 ± 0.06	3.05 ± 0.05	0.98 ± 0.10	0.33 ± 0.06	...	
118		7.14 ± 0.05	3.13 ± 0.04	0.98 ± 0.08	0.33 ± 0.05	...	
119		6.83 ± 0.06	3.56 ± 0.05	0.98 ± 0.10	0.34 ± 0.05	...	
120		6.73 ± 0.06	3.75 ± 0.06	0.95 ± 0.12	0.39 ± 0.06	...	
121		5.68 ± 0.05	3.83 ± 0.04	0.94 ± 0.08	0.41 ± 0.05	...	
122		7.32 ± 0.06	2.88 ± 0.05	1.02 ± 0.09	0.26 ± 0.06	...	
123		6.37 ± 0.05	3.67 ± 0.04	0.95 ± 0.08	0.38 ± 0.05	...	
124		6.42 ± 0.05	2.68 ± 0.04	1.01 ± 0.08	0.27 ± 0.05	...	
125		7.09 ± 0.07	3.37 ± 0.06	0.95 ± 0.12	0.39 ± 0.07	...	
126		5.99 ± 0.06	3.70 ± 0.05	0.88 ± 0.09	0.52 ± 0.06	...	
127		7.89 ± 0.12	2.42 ± 0.08	0.99 ± 0.16	0.31 ± 0.11	...	
128	IRS 24	4.84 ± 0.07	3.34 ± 0.06	1.00 ± 0.07	0.40 ± 0.08	...	
129		6.59 ± 0.06	2.79 ± 0.05	0.97 ± 0.09	0.35 ± 0.06	...	
130		7.25 ± 0.06	3.18 ± 0.05	0.96 ± 0.09	0.37 ± 0.06	...	
131		6.26 ± 0.05	2.65 ± 0.04	1.04 ± 0.08	0.23 ± 0.05	...	
132		6.98 ± 0.05	3.27 ± 0.04	0.95 ± 0.08	0.38 ± 0.05	...	

TABLE 4—*Continued*

ID	Name	K_0[a]	A_K[b]	$(J-K)_0$[a]	$(H-K)_0$[a]	$(K-L)_0$[a]	Notes
133.....		5.72 ± 0.05	3.48 ± 0.04	0.92 ± 0.08	0.44 ± 0.05	...	
134.....		8.07 ± 0.05	2.32 ± 0.04	1.06 ± 0.08	0.20 ± 0.05	...	
135.....	OSU C4	7.00 ± 0.08	3.67 ± 0.07	...	0.36 ± 0.06	...	
136.....	IRS 23	5.10 ± 0.05	3.44 ± 0.04	0.98 ± 0.06	0.46 ± 0.06	...	
137.....		7.21 ± 0.06	2.97 ± 0.05	1.00 ± 0.09	0.30 ± 0.06	...	
138.....		7.61 ± 0.08	2.78 ± 0.07	1.60 ± 0.12	0.90 ± 0.08	...	
139.....		7.50 ± 0.05	2.38 ± 0.04	1.03 ± 0.08	0.24 ± 0.05	...	
140.....		6.50 ± 0.05	2.93 ± 0.04	0.99 ± 0.08	0.31 ± 0.05	...	
141.....		7.46 ± 0.05	2.77 ± 0.04	1.02 ± 0.08	0.26 ± 0.05	...	
142.....		7.07 ± 0.05	2.84 ± 0.04	0.97 ± 0.08	0.35 ± 0.05	...	
143.....		7.32 ± 0.05	2.54 ± 0.04	1.01 ± 0.08	0.28 ± 0.05	...	
144.....		7.37 ± 0.06	2.93 ± 0.05	1.00 ± 0.09	0.30 ± 0.06	...	
145.....		5.91 ± 0.09	4.54 ± 0.09	...	0.41 ± 0.08	...	
146.....		6.54 ± 0.07	3.91 ± 0.06	0.93 ± 0.14	0.42 ± 0.07	...	
147.....		7.61 ± 0.06	2.22 ± 0.05	1.04 ± 0.09	0.22 ± 0.06	...	

NOTES—There is a one-to-one correspondence between star IDs in Table 1 and Table 4. Label "B" refers to a (usually) fainter source close to the primary source. Earlier, lower resolution data likely included both components as a single source. DS91 *J*, DS91 *H*, and DS91 *JH* refer to stars where the DS91 *J* and/or *H* magnitudes were used because no OSIRIS value was available. Please see Table 1 for notes regarding individual source identifications and spectral characteristics.

[a] Includes photometric uncertainty and uncertainty in derived A_K. K_0 results from average of DS91 and OSIRIS *K* when these differed by less than 0.2 mag.

[b] Includes photometric uncertainty only. No uncertainty given for the case of mean reddening ($A_K = 3.58$) or A_K = lower limit; see notes c and d. For the case of two or more observed colors, only observed colors that fell within ±0.5 mag of the reddening line were used to determine A_K; see text.

[c] A_K is an estimated lower limit resulting from $H-K$, where H is taken as the limiting H magnitude (14.25); see text.

[d] Mean A_K adopted from stars with measured $H-K$ only; see text.

[e] See notes for Table 1. Since this star is variable and *K* and *L* were observed at different times, it is possible that the observed $K-L$ is too red and A_K overestimated. The source is probably quite red, however, since it was not detected at *H* or *J*.

observed magnitudes that are too bright by 0.25–0.75 mag because of chance alignment or image crowding, but this can still not produce as many bright stars as are observed in the GC.

Stars with extremely red observed colors in the GC may be intrinsically redder than we have assumed. This means their derived color excess is too large, their A_K is overestimated, and their dereddened flux is too bright. In BW, the average LPV has $(H-K)_0 \sim 0.6$ mag (FW87). Such stars would have A_K overestimated in our analysis by 0.5 mag. However, such stars are also expected to be rare. Approximately 6% of the stars in the FW87 luminosity function

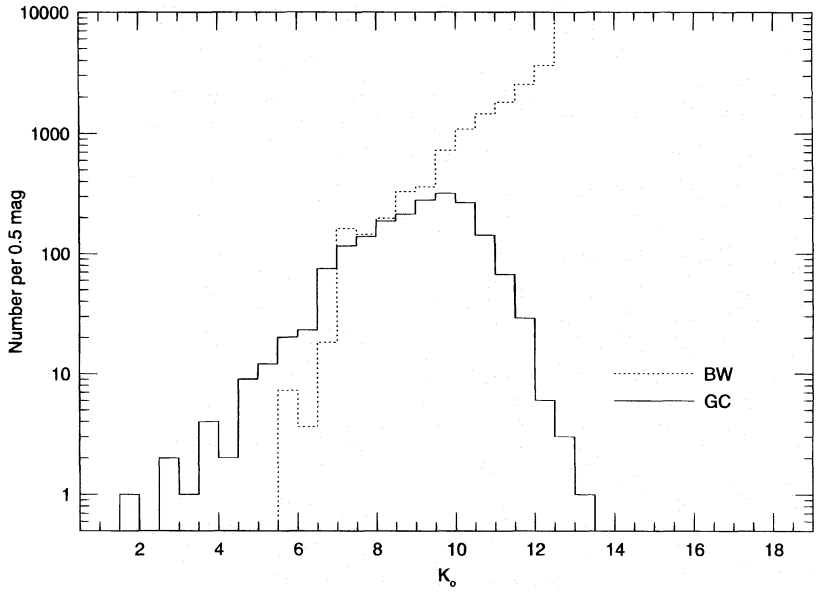

FIG. 8.—Dereddened *K*-band luminosity function for the central ~2′ of the Galaxy (*solid histogram*). The Galactic center shows a significant excess of bright stars relative to the renormalized Baade's window (*dashed line*) luminosity function. The normalization of the Baade's window luminosity function is based on the observed *K* luminosity of the GC and is also consistent with putting all the dynamically observed mass of the GC into a population with a mass-to-light ratio like that of the population in Baade's window; see text.

with $K_0 \leq 7.5$ mag are LPVs. A number of the brightest stars in Figure 8 that have large values of A_K (and $K_0 \leq 7$) estimated from only one color (several using the H-band limiting magnitude) have very red near-infrared spectra that are nearly featureless or show emission lines (IRS 3, 6E, 21, 29N). We have argued above that such stars may have excess emission and redder intrinsic colors. If this is the case, then the estimated A_K is too large and K_0 too bright. IRS 3 has a value of $A_K = 9.94$ mag, which results in $K_0 = 0.84$. This would imply a K luminosity that is much too high (consequently, IRS 3 is not plotted in Fig. 8). Two other stars detected only at K and L and having no published spectra (IRS 2L and 10EL) also have large A_K and bright K_0 (<4 mag). This small number of stars with potentially redder intrinsic colors does not change our conclusion that there is a brighter component to the KLF in the GC than seen in BW.

The fraction of *observed* flux for stars with $K_0 \leq 7$ mag is $\sim 25\%$ of the total. If we consider the integrated *dereddened* flux of the brightest stars in the KLF, we find that those with $K_0 \leq 7.0$ mag contribute approximately 65% of the total (excluding IRS 2L, 3, 6E, 10EL, 21, and 29N). This larger percentage likely results from our sensitivity limits. As stars are observed through larger A_K, only the most luminous ones will be detected. The intrinsically less luminous stars at large A_K are not detected and so contribute little to the dereddened total flux, which depends on the mean A_K of stars detected at two or more wavelengths.

Figure 6 suggests that many stars in the GC have A_K up to 4.0 mag. Since these stars all have two measured colors and many fall on or near the reddening line, we can be assured that some stars, at least, have reddening this high. If we limit all stars in the KLF to $A_K \leq 4.0$ mag, then the fraction of dereddened flux in stars with $K_0 \leq 7$ mag is approximately 30%. For BW, the fraction of flux due to stars with $K_0 \leq 7.0$ mag is 6%.

Thus, for even the most conservative limits on reddening, there is strong evidence for a brighter component to the GC KLF than exists in the KLF of the older population in BW. These excess stars, at least, we expect are the result of more recent star formation epochs (i.e., their brightness suggests they are more massive, and hence younger, than the BW stars). However, the majority of stars in this excess component do not yet have spectroscopic identifications, so it is difficult to attribute the excess to either the most recent starburst episode or one or more older one(s). The more massive emission-line stars (see the references in § 1) are relatively inconspicuous by their estimated K_0 (Table 4) or observed K (Table 1). Of the emission-line stars that have been identified spectroscopically and attributed to the most recent star formation in the GC (Krabbe et al. 1995), only eight of 149 have $K_0 \leq 7$ mag. Of these, two (IRS 6E and 29N) have only one color observed and may have infrared excess emission (see above and § 3.3) and, thus, estimated K_0 that are too bright. By contrast, 18 cool stars with $K \leq 7.0$ mag are identified by their spectra. Eleven of these have two colors measured, and all but one have H and K, so their A_K values should be reliable. At least one of these stars (IRS 7) is an M supergiant (LRT; Sellgren et al. 1987). The remaining stars may be bright giants on the AGB (LPVs); some may be supergiants. A major focus of Paper II will be an attempt to discriminate between the red supergiants and potential AGB stars because these stars trace different epochs of star formation. Two of the brightest cool stars (IRS 9 and 12N) may be LPVs based on their K-band spectra (Paper II) and large-amplitude photometric variability (§ 2.2).

The excess of bright stars at K in the GC relative to BW has important implications for the mass distribution in the GC. Clearly, the M/L ratio must change between BW and the GC. This change affects the relative distribution of mass near the GC in compact and extended components inferred from kinematics. If the stellar population is dominated by low-mass stars, as in BW, but the light is enhanced by a relatively few bright stars, the M/L ratio will be smaller than typically assumed, and the amount of mass inferred to be in a compact object would be even greater (McGinn et al. 1989; Sellgren et al. 1990; Krabbe et al. 1995; Haller et al. 1996). On the other hand, recent star formation episodes biased toward high-mass star formation near the GC may have resulted in forming a more compact cluster of stars and stellar remnants superimposed on the extended old population (Allen 1994), resulting in a M/L ratio which is larger than typically assumed. Our GC KLF only demonstrates the minimum excess of very bright stars. It cannot be used to separate the entire young population, so it is difficult to quantify this latter possibility. A recent analysis of available surface brightness and kinematic data (Saha, Bicknell, & McGregor 1996) suggests an extended mass distribution with $M/L \gtrsim 2$ inside 0.2 pc could explain the GC kinematic data without a black hole.

An excess of luminous stars in the Galactic center has been observed previously. Lebofsky & Rieke (1987), Rieke (1987, 1993), Haller & Rieke (1989), and Haller (1992) reported an excess of luminous stars in the Galactic center, relative to the luminosity function in BW. Our data are of higher spatial resolution and so are perhaps less susceptible to crowding problems (but by no means completely unaffected). In addition, we have established an upper limit to the contribution of the old stellar population in the GC by assuming its KLF is similar to that for BW and accounts for all the dynamically inferred mass in the GC.

DePoy et al. (1993b), in their study of the KLF in BW, showed that observations of this stellar population at lower spatial resolution, corresponding to higher stellar surface densities and/or larger distances, led to blending of groups of stars that would then be falsely identified as single, more luminous stars. The tests described in § 2.3 show that this is not a significant problem in the GC at our spatial resolution. Our experiments showed no significant number of spurious detections of bright stars created by chance groupings. Thus, the excess of luminous stars in the KLF is real and not an artifact of image crowding.

4. SUMMARY

We have presented near-infrared photometry for approximately 2000 stars in the central ~ 5 pc of the Galaxy. The $J-H$ versus $H-K$ color-color diagram and K versus $J-K$, $H-K$ CMDs demonstrate the large and variable interstellar extinction toward the GC. Combinations of $J-H$, $H-K$, and $K-L$ colors were used to estimate the near-infrared extinction, A_K, for approximately 1100 stars. Analysis of the observed colors shows that the majority of stars are likely to have intrinsic colors similar to bulge or field giants seen through 2–4 mag of extinction (A_K). While the mean A_K for stars with one or more observed colors is approximately 3.3 mag, we show that there are likely stars for which A_K is much higher ($A_K > 6$ mag in some cases).

Some GC objects may have excess circumstellar emission. Potential excesses are seen in stars that are possibly pre–main-sequence objects (IRS 1W, IRS 21) and also in post–main-sequence objects (IRS 6E), analogous to possibly similar objects elsewhere in the Galaxy. The potential pre–main-sequence objects are compared to well-studied young stellar objects; these objects may have similar near-infrared luminosities and colors as the GC objects depending on their circumstellar versus interstellar reddening.

Our J-band photometry confirm the variability of several stars noted by previous investigators (IRS 9 and 12N), and our J, H, K, and 2.2 μm photometry clearly establishes the variability of the well-known M supergiant, IRS 7.

Our dereddened photometry was used to construct a K-band luminosity function that confirms the excess of bright stars in the GC relative to the old stellar population in Baade's window pointed out in previous work. Our KLF is constructed from higher spatial resolution observations than earlier work, and we demonstrate that the excess cannot be due to image crowding. Approximately 25% of the observed flux in the GC comes from stars that comprise a brighter component to the GC stellar population than found in the old stellar population in Baade's window. The majority of stars in this component ($K_0 \leq 7.0$ mag) with spectral identifications are cool stars. By contrast, the massive, emission-line stars are less conspicuous in this component. It remains to be seen whether the majority of the brightest cool stars trace the most recent star formation in the GC (<10 Myr) or somewhat older star formation ($\gtrsim 100$ Myr). Two of the brightest cool stars (IRS 9 and 12N) have near-infrared spectra (Paper II) and photometric variations suggestive of LPVs.

This work was supported by National Science Foundation grants AST 90-16112, AST 91-15236, and AST 92-18449. Support for this work was also provided by NASA through grant number HF 01067.01-94A from the Space Telescope Science Institute, which is operated by the Association of Universities for Research in Astronomy, Inc., under NASA contract NAS5–26555. We wish to thank J. Holtzman for providing us with his modified DAOPHOT routines and useful discussions regarding crowded field photometry. Our work has also benefited from discussions on crowded field photometry with G. Tiede and L. Kuchinski. We are grateful to J. Frogel for observing IRS 7 for us in 1995 April. We kindly thank M. Werner for communication of results prior to publication. We also thank an anonymous referee whose comments have resulted in a clearer presentation.

APPENDIX

Here we present details of our comparison to the images of DS91 and compare our OSIRIS K-band photometry to recent values given in the literature. Comparison of all DS91 and OSIRIS magnitudes matched at J, H, or K results in rms differences of 0.21, 0.23, and 0.18 mag for ΔJ, ΔH, and ΔK, respectively. Here four of 28, five of 32, and four of 57 stars with differences greater than 2 σ were excluded at J, H, and K, respectively. At J and H, the rms is about twice an average DAOPHOT error for these same stars. At K the rms is similar to an average DAOPHOT error. The difference at J and H may be larger because of the smaller PSF radius than for the K frames. This would affect fainter stars more. Plots of ΔJ versus J and ΔH versus H suggest that this is the case. Therefore, we include the DS91 photometry in our analysis in the following way: we have averaged the K data from the DS91 data set with our OSIRIS data set for stars that have ΔK less than 0.2 for purposes of deriving A_K and computing the K-band luminosity function. However, we present the observed DS91 and OSIRIS data separately in Table 1. The DS91 J and H data were used for estimating A_K with OSIRIS data for stars that have ΔK less than 0.2 if no OSIRIS J or H magnitude was measured.

We have compared our derived K magnitudes with the average K magnitudes of Simons et al. (1990) and Simon et al. (1990) and find excellent agreement for the four bright IRS 16 sources (C, NE, NW, SW). These K magnitudes were derived from high ($<0\farcs05$) spatial resolution lunar occultation measurements. The difference between the OSIRIS K magnitudes and the average of the Simons et al. (1990) and Simon et al. (1990) data (as reported by Simons et al. 1990) is 0.02 ± 0.13 mag, where the uncertainty given is the standard deviation.

The OSIRIS K magnitudes are consistent, within the uncertainties, with those presented by Tollestrup et al. (1989), with OSIRIS fainter by 0.32 ± 0.60 mag (IRS 1NE, 1SE, 16NE, 16NW, 16SW, 16C, 16SW-E = MPE + 1.6 − 6.8 compared). Tollestrup et al. used single-source PSF fitting to derive point-source magnitudes from their $\lesssim 1$–$1\farcs5$ images.

Tamura et al. (1996) present K magnitudes for 26 stars in common with the OSIRIS data set. Their $0\farcs9$ synthesized aperture photometry is systematically brighter than the OSIRIS data by 0.40 ± 0.40 mag (comparing OSIRIS to the Tamura et al. 1993 August data). The uncertainty is the standard deviation, as above. For the large number of stars compared, the uncertainty in the mean is considerably smaller (± 0.08 mag). This is expected since the Tamura et al. data did not include background subtraction and the synthesized apertures can suffer from contamination by other stars (Tamura et al. were primarily looking for relative variations).

The OSIRIS K magnitudes are systematically fainter than those derived by Rieke et al. (1989). For six stars in common (IRS 10E, 10W, 13E, 16NE, 16NW, 16SW), we find a difference of 0.85 ± 0.30 mag. The Rieke et al. photometry was derived from synthesized apertures on their low spatial resolution images ($\lesssim 1\farcs5$), which is consistent with the somewhat brighter magnitudes.

We also find that the OSIRIS K magnitudes are systematically faint compared to those reported by Krabbe et al. (1995) for 11 bright sources in the central $\sim 10''$ (IRS 6E, 13E, 15SW, 16C, 16NE, 16NW, 16SW, 29N, 33E, AF, MPE + 1.6 − 6.8). The difference in K for these 11 sources is 0.80 ± 0.31 mag. Comparing only the four bright IRS 16 sources, as for the lunar occultation measurements, the difference between OSIRIS and Krabbe et al. (1995) K magnitudes is 0.83 ± 0.22 mag, the values of Krabbe et al. again being brighter. Krabbe et al. (1995) actually report K magnitudes derived from the high angular resolution (deconvolved resoluti $0\farcs2$) images of Eckart et al. (1993, 1995); it is not clear how the flux scale was calibrated

or whether the magnitudes are affected by the Eckart et al. image restoration technique. If IRS 7 was used as the flux calibrator, then it is possible that this could result in some of the difference, as we find that IRS 7 is variable (see below). Krabbe et al. (1995) do note that their absolute K magnitudes appear to be 1–2 mag brighter than expected for stars of similar spectral type elsewhere in the Galaxy.

REFERENCES

Allen, D. A. 1972, ApJ, 172, L55
———. 1994, in Nuclei of Normal Galaxies: Lessons from the Galactic Center, ed. R. Genzel & A. I. Harris (Dordrecht: Kluwer), 293
Allen, D. A., Hyland, A. R., & Hillier, D. J. 1990, MNRAS, 244, 706
Allen, D. A., Hyland, A. R., & Jones, T. J. 1983, MNRAS, 204, 1145
Bailey, M. E. 1980, MNRAS, 190, 217
Becklin, E. E. 1995, in IAU Symp. 169, Unsolved Problems in the Milky Way, ed. L. Blitz (Dordrecht: Kluwer), in press
Becklin, E. E., Mathews, K., Neugebauer, G., & Willner, S. P. 1978, ApJ, 220, 831
Becklin, E. E., & Neugebauer, G. 1967, ApJ, 147, 799
———. 1968, ApJ, 151, 145
———. 1975, ApJ, 200, L71
Beckwith, S., Evans, N. J., Becklin, E. E., & Neugebauer, G. 1976, ApJ, 208, 390
Blum, R. D., DePoy, D. L., & Sellgren, K. 1995a, ApJ, 441, 603
Blum, R. D., Sellgren, K., & DePoy, D. L. 1995b, ApJ, 440, L17
———. 1996, in preparation (Paper II)
Castelaz, M. W., Grasdalen, G. L., Hackwell, J. A., Capps, R. W., & Thompson, D. 1985, AJ, 90, 1113
Chini, R., Krugel, E., & Wargau, W. 1987, A&A, 181, 378
Cohen, M., van der Hucht, K. A., Williams, P. M., & Thé, P. S. 1991, ApJ, 378, 302
DePoy, D. L., Atwood, B., Byard, P., Frogel, J. A., & O'Brien, T. 1993a, Proc. SPIE 1946, 667
DePoy, D. L., & Sharp, N. A. 1991, AJ, 101, 1324 (DS91)
DePoy, D. L., Terndrup, D. M., Frogel, J. A., Atwood, B., & Blum, R. 1993b, AJ, 105, 2121
Eckart, A., Genzel, R., Hofmann, B., Sams, B. J., & Tacconi-Garman, L. E. 1993, ApJ, 407, L77
———. 1995, ApJ, 445, L23
Evans, N. J., Blair, G. N., & Beckwith, S. 1977, ApJ, 217, 448
Evans, N. J., Mundy, L. G., Kutner, M. L., & DePoy, D. L. 1989, ApJ, 346, 212
Figer, D. F. 1995, Ph.D. thesis, UCLA
Forrest, W. J., Shure, M. A., Pipher, J. L., & Woodward, C. E. 1987, in The Galactic Center, ed. D. C. Backer (New York: AIP), 153
Frogel, J. A., Persson, S. E, Aaronson, M., & Mathews, K. 1978, ApJ, 220, 75
Frogel, J. A., & Whitford, A. E. 1987, ApJ, 320, 199 (FW87)
Genzel, R., Hollenbach, D., & Townes, C. H. 1994, Rept. Prog. Phys., 57, 417
Hall, D. N. B., Kleinmann, S. G., & Scoville, N. Z. 1982, ApJ, 262, L53
Haller, J. 1992, Ph.D. thesis, Univ. of Arizona
Haller, J. W., & Rieke, M. J. 1989, in IAU Symp. 136, The Center of the Galaxy, ed. M. Morris (Dordrecht: Kluwer), 487
Haller, J., Rieke, M. J., Rieke, G. H., Tamblyn, P., Close, L., & Melia, F. 1996, ApJ, 456, 194
Johnson, H. 1966, AR&A, 4, 193
Krabbe, A., Genzel, R., Drapatz, S., & Rotaciuc, V. 1991, ApJ, 382, L19
Krabbe, A., et al. 1995, ApJ, 447, L95
Lacy, J. H., Townes, C. H., & Hollenbach, D. J. 1982 , ApJ, 262, 120
Lebofsky, M. J., & Rieke, G. H. 1987, in The Galactic Center, ed. D. C. Backer (New York: AIP), 79
Lebofsky, M. J., Rieke, G. H., & Tokunaga, A. T. 1982, ApJ, 263, 736 (LRT)
Libonate, S., Pipher, J. L., Forrest, W. J., & Ashby, M. L. N. 1995, ApJ, 439, 202
Lindqvist, M., Habing, H. J., Winnberg, A., & Matthews, H. E. 1992, A&AS, 92, 43
Mathis, J. S. 1990, AR&A, 28, 37
McGinn, M. T., Sellgren, K., Becklin, E. E., & Hall, D. N. B. 1989, ApJ, 338, 824
Merrill, K. M., & Stein, W. A. 1976, PASP, 88, 874
Morris, M. 1993, ApJ, 408, 496
Neugebauer, G., Becklin, E. E., Beckwith, S., Mathews, K., & Wynn-Williams, C. G. 1976, ApJ, 205, L139
Phinney, E. S. 1989, in IAU Symp. 136, The Center of the Galaxy, ed. M. Morris (Dordrecht: Kluwer), 543
Reid, M. J. 1993, AR&A, 31, 345
Rieke, G. H., Rieke, M. J., & Paul A. E. 1989, ApJ, 336, 752
Rieke, M. J. 1987, in Nearly Normal Galaxies from the Planck Time to the Present, ed. S. M. Faber (New York: Springer), 90
———. 1993, in Back to the Galaxy, ed. S. Holt & F. Verter (New York: AIP), 37
Saha, P., Bicknell G. V., & McGregor, P. J. 1996, ApJ, 449, 000
Sellgren, K., Hall, D. N. B., Kleinmann, S. G., & Scoville, N. Z. 1987, ApJ, 317, 881
Sellgren, K., McGinn, M. T., Becklin, E. E., & Hall, D. N. B. 1990, ApJ, 359, 112
Shu, F. H., Adams, F. C, & Lizano, S. 1987, AR&A, 25, 23
Simon, M., Chen, W. P., Forrest, W. J., Garnett, J. D., Longmore, A. J., Gauer, T., & Dixon, R. I., 1990, ApJ, 360, 95
Simon, M., Peterson, D. M., Longmore, A. J., Storey, J. W. V., & Tokunaga, A. T. 1985, ApJ, 298, 328
Simons, D. A., Hodapp, K. W., & Becklin E. E.1990, ApJ, 360, 106
Stetson, P. B. 1987, PASP, 99, 191
Storey, J. W. V., & Allen, D. A. 1983, MNRAS, 204, 1153
Tamblyn, P., Rieke, G. H., Hanson, M. M., Close, L. M., McCarthy, D. W., Jr., & Rieke, M. J. 1996, ApJ, 456, 206
Tamura, M., Werner, M. W., Becklin, E. E., & Phinney, E. S. 1994, in Infrared Astronomy with Arrays: The Next Generation, ed. I. McLean (Dordrecht: Kluwer), 117
———. 1996, ApJ, 449, 000
Tiede, G. P., Frogel, J. A., & Terndrup, D. M. 1995, AJ, 110, 2788
Tollestrup, E. V., Capps, R. W., & Becklin, E. E. 1989, AJ, 98, 204
Treffers, R. R., Fink, W., Larson, H. P., & Gautier, T. N. 1976, ApJ, 209, L115
Werner, M. W., Becklin, E. E., Gatley, I., Matthews, K., Neugebauer, G., & Wynn-Williams, C. G. 1979, MNRAS, 188, 463
Williams, P. M., van der Hucht, K. A., & Thé, P. S. 1987, A&A, 182, 91
Wollman, E. R., Smith, H. A., & Larson, H. P. 1982, ApJ, 258, 506
Wynn-Williams, C. G. 1982, AR&A, 20, 587